



## รายงานวิจัยฉบับสมบูรณ์

## โครงการ การผลิตเอทิลีนหรือบิวทานอลจากเอทานอลชีวภาพ ด้วยสมบัติกรดเบสของเลพิโดโครไซท์ไททาเนท

# โดย ผศ. ดร. ทศพล เมลืองนนท์

### รายงานวิจัยฉบับสมบูรณ์

## โครงการ การผลิตเอทิลีนหรือบิวทานอลจากเอทานอลชีวภาพ ด้วยสมบัติกรดเบสของเลพิโดโครไซท์ใททาเนท

ผศ. ดร. ทศพล เมลืองนนท์ สถาบันเทคโนโลยีพระจอมเกล้าเจ้าคุณทหารลาดกระบัง

สนับสนุนโดยคณะกรรมการการอุดมศึกษา และสำนักงานกองทุนสนับสนุนการวิจัย

(ความเห็นในรายงานนี้เป็นของผู้วิจัย สกอ. และ สกว. ไม่จำเป็นต้องเห็นด้วยเสมอไป)

#### **Abstract**

Project Code: MRG6080004

Project Title: Production of ethylene or butanol from bioethanol by acid-base properties

of lepidocrocite titanate

Investigator: Tosapol Maluangnont, College of Nanotechnology, King Mongkut's

Institute of Technology Ladkrabang

E-mail Address: tosapol.ma@kmitl.ac.th

Project Period: 3 April 2017 to 2 October 2019

The low return on investment for bioethanol fuel has led to its transformation to more valuable chemicals such as ethylene or butanol. While acid sites are required for ethylene production, the protonic titanates typically possess low thermal stability (< 100 <sup>o</sup>C). On the other hand, titanate-based catalysts with basic sites for butanol production have not been reported. In this work, cesium lepidocrocite titanate microcrystals Cs<sub>x</sub>Ti<sub>2-</sub>  $_{v}M_{v}O_{4}$  (x = 0.67, 0.70; M =  $\square$ , Zn) were prepared and tested for ethanol conversion at 380 °C. These catalysts were characterized regarding the long range- and localstructure, thermal stability, morphology, elemental compositional distribution, and acidicbasic properties. Relevant materials such as protonic lepidocrocite titanate, anatase-type TiO<sub>2</sub>, zeolite HZSM-5 and MgO were also compared. The observed ethylene clearly indicates the active acid sites, while butanol (which requires the basic sites) was minimally produced. Therefore, cesium lepidocrocite titanates explored herein are the rare examples of acidic cesium-containing material. The low ethanol conversion can be increased by ball milling, which decreases the particle sizes and therefore increases a surface area. Moreover, these titanates were structurally stable in a harsh environment at least up to 800  $^{\circ}$ C under dry NH $_{3}$ , and 380  $^{\circ}$ C under the mixture of ethanol feed and water by-product. This temperature range is significantly higher than that at 100 °C normally employed for protonic titanate, opening up a possibility in other highertemperature applications catalyzed by acid sites.

Keywords: bioethanol, ethylene, lepidocrocite titanate, acid strength and acidity

#### บทคัดย่อ

หมายเลขโครงการ: MRG6080004

ชื่อโครงการ: การผลิตเอทิลีนหรือบิวทานอลจากเอทานอลชีวภาพด้วยสมบัติกรดเบสของ

เลพิโดโครไซท์ไททาเนท

Investigator: ทศพล เมลืองนนท์, วิทยาลัยนาโนเทคโนโลยีพระจอมเกล้าลาดกระบัง, สถาบัน

เทคโนโลยีพระจอมเกล้าเจ้าคุณทหารลาดกระบัง

อีเมลล์: tosapol.ma@kmitl.ac.th

ระยะเวลาดำเนินการวิจัย: 3 เมษายน 2560 ถึง 2 ตุลาคม 2562

ผลตอบแทนต่ำจากการลงทุนเพื่อผลิตเชื้อเพลิงเอทานอลชีวภาพ ได้นำไปสู่การศึกษาเพื่อ เปลี่ยนเป็นสารเคมีอื่นที่มีราคาสูงขึ้นเช่นเอทิลีนหรือบิวทานอล การผลิตเอทิลีนต้องการตำแหน่ง กรด แต่ไททาเนทที่มีโปรตอนมักมีความเสถียรทางความร้อนต่ำ (น้อยกว่า 100 °C) ในทาง กลับกันยังไม่มีรายงานเกี่ยวกับตัวเร่งปฏิกิริยาไททาเนทที่มีตำแหน่งเบส สำหรับการผลิตบิวทา-งานวิจัยนี้ได้เตรียมผลึกระดับไมโครเมตรของซีเซียมเลพิโดโครไซท์ไททาเนท Cs<sub>x</sub>Ti<sub>2-</sub>  $_{v}$ M $_{v}$ O $_{4}$  (x = 0.67, 0.70; M =  $\square$ , Zn) และทดสอบการเปลี่ยนเอทานอลที่ 380  $^{\circ}$ C  $_{v}$  ตัวเร่ง ปฏิกิริยาเหล่านี้ได้รับการพิสูจน์ลักษณะทั้งโครงสร้างในระยะไกลและระยะใกล้ ความเสถียรทาง ความร้อน สัณฐาน การกระจายตัวขององค์ประกอบธาตุ และสมบัติกรด-เบส วัสดุที่เกี่ยวข้อง เช่น ไททาเนทที่มีโปรตอน ไททาเนียมไดออกไซด์แบบนาเทส ซีโอไลต์ ZSM-5 และแมกนีเซียม เอทิลีนที่ถูกตรวจพบแสดงให้เห็นชัดเจนว่ามีตำแหน่งกรด ออกไซด์ได้รับการทดสอบเช่นกัน ในขณะที่บิวทานอล(ซึ่งต้องการตำแหน่งเบส)ถูกผลิตขึ้นในปริมาณน้อย ดังนั้นซีเซียมเลพิโดโคร ไซท์ไททาเนทซึ่งได้รับการสำรวจในงานนี้ เป็นตัวอย่างที่หาได้ยากของวัสดุที่มีซีเซียมและเป็น กรด พบว่าการเปลี่ยนเอทานอลที่ต่ำนั้นอาจเพิ่มขึ้นได้โดยการบดย่อยด้วยลูกบอล ซึ่งลดขนาด อนุภาคลงและดังนั้นจึงเพิ่มพื้นที่ผิวขึ้น นอกจากนี้ ไททาเนทเหล่านี้เสถียรทางโครงสร้างใน ัสภาพแวดล้อมที่รุนแรงคือ ที่อุณหภูมิไม่น้อยกว่า 800 °C ภายใต้ก๊าซแอมโมเนียที่แห้ง และไม่ น้อยกว่า 380 °C ภายใต้ของผสมของเอทานอลที่เป็นสารตั้งต้นและน้ำที่เป็นผลิตภัณฑ์พลอย ได้ ช่วงอุณหภูมินี้สูงขึ้นอย่างมีนัยสำคัญกว่าอุณหภูมิ 100 °C ที่มักใช้กันทั่วไปในไททาเนทที่มี โปรตอน และได้เปิดโอกาสในการประยุกต์ใช้อื่นที่ต้องการตำแหน่งกรดและที่อุณหภูมิสูง

**คำสำคัญ:** เอทานอลชีวภาพ, เอทิลีน, เลพิโดโครไซท์ไททาเนท, ความแรงของกรดและความ เป็นกรด

#### **Executive Summary**

The conversion of ethanol to more valuable chemicals such as ethylene or butanol is of interest nowadays. Common acidic materials catalyzing the ethanol-to-ethylene transformation include protonic titanate which unfortunately has low thermal stability (<  $100^{\circ}$ C). On the other hand, titanate-based materials with basic sites for ethanol-to-butanol conversion are not well known. This project reported the cesium lepidocrocite titanates  $Cs_xTi_{2-y}M_yO_4$  (x = 0.67, 0.70; M =  $\square$ , Zn) as the rare examples of acidic cesium-containing titanium oxides, since  $Cs^+$  is generally believed to promote the basic character. The ethanol-to-ethylene conversion clearly indicates the active acid sites, while butanol (requiring basic sites) was minimally produced. The low ethanol conversion can be improved by ball milling. Importantly, the cesium lepidocrocite titanates were stable in several types of harsh environment (380-800  $^{\circ}$ C), significantly higher than 100  $^{\circ}$ C normally employed for protonic titanate.

### Content

Abstracti
บทคัดย่อii
Executive Summaryi
1. Objectives
2. Introduction
3. Methodology
3.1) Synthesis
3.2) Characterization
3.3) Temperature-programmed desorption
3.4) Catalytic activity testing10
4. Results and Discussion11
4.1) Structural characteristics1
4.2) Thermal stability1
4.3) Acid strength and acidity18
4.4) Possible nature of acid sites
4.5) Catalytic activity
5. Conclusion and suggestions
6. References4
7. Output

### Content (continued)

### **Appendix**

- A1. ผลงานตีพิมพ์ที่ได้จากโครงการ
- A2. แบบสรุปปิดโครงการและการนำผลจากโครงการไปใช้ประโยชน์
- A3. สรุปรายงานการเงิน
- A4. หนังสือนำส่งรายงานฉบับสมบูรณ์
- A5. หนังสือขออนุมัติเปลี่ยนชื่อโครงการ
- A6. หนังสือขออนุมัติขยายเวลาโครงการวิจัย
- A7. Permission/license to reproduce the published work

#### 1. Objectives

- 1.1) To synthesized selected compositions of alkali lepidocrocite titanate via a traditional solid state synthesis method. The compositions studied include  $Cs_xTi_{2-x/4}\square_{x/4}O_4$  (x=0.70 and 0.67),  $Cs_xZn_{x/2}Ti_{2-x/2}O_4$  (x=0.70) and  $K_xZn_{x/2}Ti_{2-x/2}O_4$  (x=0.80). These compositions vary in the number of negative charge per formula unit (x, 0.7 vs 0.8), the content and electronegativity of the metal component (x in the presence of x in the content and lastly the type of the interlayered alkali ions (x in the content x in the content x in the presence of x in the content x
- 1.2) To characterize the prepared materials in several aspects including structural chemistry at both local- and long-range, thermal stability, morphology, compositional distribution, and acidic-basic properties. Techniques utilized included X-ray diffraction (XRD), X-ray photoelectron spectroscopy (XPS), Raman spectroscopy, X-ray fluorescence spectrometry (XRF), energy-dispersive X-ray spectroscopy (EDX), scanning electron microscopy (SEM), thermogravimetric analysis (TGA), N<sub>2</sub> adsorption/desorption, NH<sub>3</sub> and CO<sub>2</sub>-temperature programmed desorption (TPD), and infrared (IR) spectroscopy of sorbed pyridine; and to compare the acidic properties (amount and strength) with more widely-studied materials such as protonic titanate, TiO<sub>2</sub>, zeolite HZSM-5, and MgO.
- 1.3) To evaluate the catalytic activity of the synthesized materials in ethanol conversion, in relation to some of the common metal oxides; and to correlate the ethanol conversion and product selectivity to the characterized physicochemical properties including the acidic-basic properties.

#### 2. Introduction

The low return on investment for bioethanol *fuel* has recently challenged its economic profitability. <sup>1,2</sup> So, the chemical conversion of bioethanol into more valuable *chemicals* is under intense investigation. <sup>3</sup> The transformation of the relatively inexpensive bioethanol (*i.e.*, derived from sugar and starch based crops) to value-added chemicals could contribute to the economic growth and sustainable social welfare of Thailand. The chemistry involved is mainly the dehydration of ethanol to ethylene which is catalyzed by acid sites. On the other hand, other reactions require the basic sites <sup>4</sup> such as the ethanol-to-butanol conversion.

This report summarized the production of ethylene from bioethanol via the acid property of a class of materials called lepidocrocite titanate. Recently, layered-type potassium lepidocrocite titanate has emerged as a new basic catalyst in the conversion of fatty acid into renewable fuel. This transformation had been previously supported by TRG5780160 to the current investigator, and the results  $^{5,6}$  can be found in the literature. Lepidocrocite titanate is a layered metal oxide of the general composition  $A_xM_yTi_{2-y}O_4$ . The metals M reported in the literature are of different valency such as +1 (Li),  $^8$  +2 (Mg, Co, Ni, Cu, Zn),  $^{9,10,11}$  +3 (Sc, Al, Fe, Mn),  $^{12}$  +5 (Nb),  $^{13}$  or even the titanium vacancy (denoted by the symbol  $\square$ ). Such aliovalent substitution of M for  $Ti^{4+}$  gives rise to the negative charge in the sheets. To preserve charge neutrality, the alkali cations A situate in the interlayer space. There was a linear correlation  $^6$  between the yield of the liquid hydrocarbons vs the calculated negative charges of the oxygen atom (acting as the basic site) in  $K_xM_yTi_{2-y}O_4$ , providing a solid evidence that the internal basic sites are essential in such transformation. Building from this knowledge, it was first expected that

the *cesium* lepidocrocite titanate would be basic, catalyzing the ethanol-to-butanol conversion. Actually, it is reported herein the rather unusual *acidic* property of some compositions of the cesium lepidocrocite titanate; such property can be adequately rationalized based on its solid state and surface chemistry, including the electronegativity of the metal component, the morphology (*i.e.*, surface area), and also the activation temperature prior to the measurements.

Acidic materials either of Brønsted- (proton-donating) or Lewis-type (electron-accepting) are of paramount importance in industrial hydrocarbon chemistry, <sup>15</sup> biomass conversion and fine chemicals synthesis. <sup>16,17,18</sup> Recently, *protonic* layered metal oxides (e.g., titanates, niobates) have received increasing attention due to their compositional, structural, and microstructural tunability. <sup>19,20,21</sup> The *Brønsted* acidic properties rely on the two-dimensional (2D) nature, where protons from the medium exchange with the interlayer cations and are incorporated at the gallery. On the other hand, the *Lewis* acidic properties originated from the electron-deficient species, either at the interlayer or at the sheets, have been much less explored.

To prepare 2D materials with Brønsted acid sites accessible to probe molecules or reactants, proton exchange of such solids is typically followed by pillaring, <sup>22,23</sup> delamination, <sup>24</sup> and restacking; <sup>19</sup> or the synthesis is conducted in the presence of a structure directing agent. <sup>25</sup> Otherwise, they typically exhibit low acidity as a result of relatively large particles often in the form of microcrystals. In addition, the low thermal stability of the layered structure containing Brønsted sites limits the application window to a relatively mild reaction temperatures, mostly  $<100^{\circ}$ C. <sup>26,27,28,29,30</sup> For example, Sasaki *et al* reported <sup>31</sup> that the lepidocrocite-type  $H_xTi_{2-x/4}\square_{x/4}O_4$   $H_2O$  (x = 0.7,  $\square$  = Ti

vacancy;  $H_{0.7}TO$ ) layered crystals transformed to anatase at 450  $^{\circ}C$  with an extensive mass loss of ~15 wt%. If the protonic form was pillared with aluminum polyoxocations, the layered structure was stable up to 500  $^{\circ}C$ , at which Brønsted acid sites disappeared while Lewis acid sites remained. Similar decomposition and layered collapse was also observed in the structurally-related  $H_2Ti_3O_7$  nanotubes.

These shortcomings in protonic layered titanates prompt the exploration of developing a proton-free, Lewis acidic material. It is well known that lepidocrocite-type alkali titanate  $^{14,32,12,33}$  is structurally robust, and that the 2D layered structure is preserved even when heated  $\sim 100$  °C above the synthetic temperature.  $^{34}$  Lepidocrocite titanate has the general composition  $A_xTi_{2-y}M_yO_4$  (i.e.,  $xA^+(Ti_{2-y}M_yO_4)^x$ ), where x=y(4-n) is the nominal charge per formula unit; n<4 is the oxidation state of M, and n=0 for  $M=\square$ . In this structure, the corrugated double edge-shared (Ti,M)O<sub>6</sub> octahedra join into negatively-charged sheets, extend through the ac (basal) plane, and stack along the b-direction. The sheets are staggered such that  $b=2\times d_{020}$ , with  $A^+$  ions situated at the interlayer space, see Figure 1. The Ti,M atoms potentially serves as the Lewis acid sites especially if they are on the accessible surfaces.

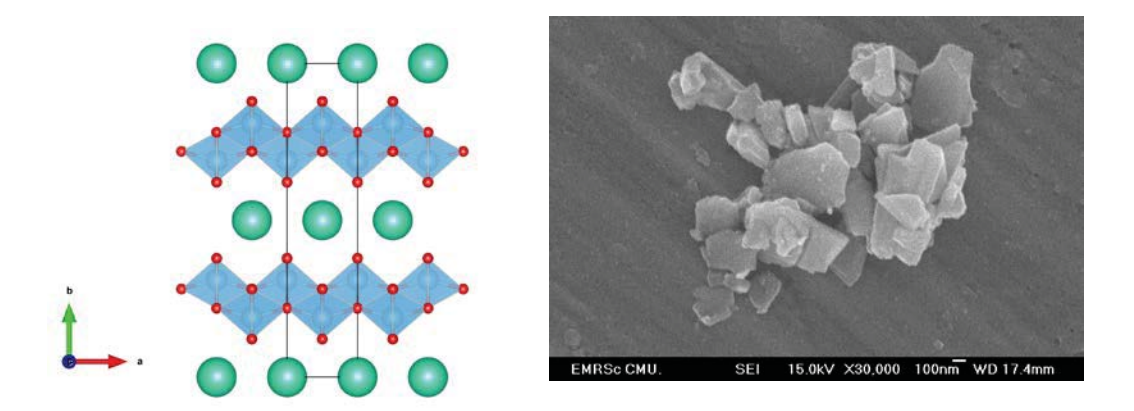


Figure 1. (Left) crystal structure of  $A_x Ti_{2-y} M_y O_4$  (drawn with VESTA<sup>35</sup>) shown as the polyhedra representation on the *ab* plane; (right) a representative SEM image of  $Cs_{0.7}TO$  with the scale bar indicating the distance of 100 nm.

At the beginning of this project, it was assumed that the acidic nature of a proton-free lepidocrocite titanate could be tuned by the inductive effect of both M at the sheets and the interlayer A cations. If so, a Lewis acidic material (*i.e.*, relative to the pristine, unmodified composition) capable of withstanding high temperature (relative to the protonic form) might be obtained. Reports on such modifications, however, are rather limited. Relevant examples include the ion exchange of H<sub>0.7</sub>TO with aqueous solution of the metal ions, <sup>36</sup> or the deposition of metal nanoparticles onto the surfaces of H<sub>2</sub>Ti<sub>3</sub>O<sub>7</sub> nanotubes. <sup>37</sup> Yet, the enhanced acidic nature has not been fully demonstrated.

Quite unexpectedly, it was found that the *cesium* titanate  $Cs_xTi_{2-x/4}$   $\square_{x/4}O_4$  (x = 0.67, 0.70; M =  $\square$ ;  $Cs_xTO$ ) and  $Cs_xTi_{2-x/2}Zn_{x/2}O_4$  (x = 0.70;  $Cs_{0.7}ZnTO$ ), directly obtained right after the solid state synthesis, was unusually acidic without the need for proton/ion exchange, pillaring, delamination, or restacking. These results provide an interesting example contrasting the general view that soft/polarizable cesium ions

suppress acidic- while promoting basic-characters. Acidity and acidic nature of the microcrystals of these compositions was evaluated by NH $_3$  and isopropylamine-TPD, FTIR of adsorbed pyridine, and XPS. Effects of the Ti vacancy sites and activation temperature on acidity, including the stability of the cesium titanate, were also investigated. Consistent with the observed acid function, catalytic activity of the cesium titanate  $Cs_xTi_{2-x/4}\square_{x/4}O_4$  toward conversion of ethanol was highlighted.

#### 3. Methodology

#### 3.1)Synthesis

The samples were prepared following the reported procedure,  $^{31,32,33}$  by first calcining the stoichiometric mixture of  $A_2CO_3$  (A = K or Cs), anatase-type  $TiO_2$ , and ZnO (when necessary) at 800 °C for 1 h for decarbonation. Next, the mixture was ground and subjected to two cycles of calcination (20 h each) at 800 °C ( $Cs_{0.7}Ti_{1.825}\Box_{0.175}O_4$ ,  $Cs_{0.7}TO$ ),  $^{31}$  900 °C ( $K_{0.8}Zn_{0.4}Ti_{1.6}O_4$ ,  $K_{0.8}ZnTO$ ),  $^{32}$  or 950 °C ( $Cs_{0.7}Zn_{0.35}Ti_{1.65}O_4$ ;  $Cs_{0.7}ZnTO$ ),  $^{33}$  all with intermediate grinding. These were hereafter called "as made" and they were used for characterization and catalytic activity testing.

Proton exchange of  $Cs_{0.7}TO$  to  $H_{0.7}Ti_{1.825}\square_{0.175}O_4\cdot H_2O$  ( $H_{0.7}TO$ ) was done three times at room temperature with 1 M HCI, following the reported method <sup>31</sup> with the acid renewed everyday. The solid-to-solution was fixed at 1 g-to-100 mL. The solid was washed with deionized water until it was free from excess acids. The resulting material was dried overnight at RT.

To study the effect of the particle size on acidity, two additional samples were prepared. For  $Cs_{0.7}TO$ -BM (BM for ball-milled), ~8.0 g of  $Cs_{0.7}TO$  was mixed with zirconia balls in a 500 mL bottle such that the volume of the balls is 2/3 of the bottle. Ethanol was filled until it completely covered the powder. The milling was continuously performed at 6,500 rpm for 18 h. After that, the powder was separated from the balls, washed, and dried overnight at 120 °C. In another sample, the  $Cs_{0.67}Ti_{1.8325}\square_{0.1675}O_4$  ( $Cs_{0.67}TO$ ) was directly prepared via solid state synthesis (as for  $Cs_{0.7}TO$ ) but using the nanosized P25  $TiO_2$  (Degussa, 99.70%)<sup>42</sup> as the Ti source instead of anatase, to increase the specific surface area.

#### 3.2) Characterization

X-ray diffraction (XRD) measurements were performed on a Rigaku, DMAX 2200/Ultima+ diffractometer (Cu K $\alpha$  radiation, 40 kV, 30 mA). Unit cell parameters were refined using the program CellCalc.  $^{48}$  The specific surface area  $S_{\rm BET}$  was measured by an Autosorb-1C instrument (Quantachrome). Bulk elemental composition was analyzed using either a Rigaku ZSX Primus IV wavelength dispersive X-ray fluorescence (WD-XRF) spectrometer, or an Oxford X-Max<sup>N</sup> 20 Energy-dispersive X-ray (EDX) analyzer inside a Zeiss EVO MA10 scanning electron microscope. The latter was also used for scanning electron microscopic (SEM) investigation. XPS measurements were conducted SUT-NANOTEC-SLRI XPS workstation 5000 (PHI monochromatized Al K $\alpha$  radiation at 1486.6 eV), with the binding energies calibrated to C1s at 284.8 eV. The analysis area is 300 × 300  $\mu$ m<sup>2</sup>. Thermogravimetric (TG) analysis was performed under the flow of N<sub>2</sub> gas (20 mL·min<sup>-1</sup>) from RT to 700 °C (10 °C·min<sup>-1</sup>) using a Perkin-Elmer, Pyris-1 instrument. The IR spectra were directly acquired from the powder in the attenuated total reflectance (ATR) mode using a PerkinElmer, Spectrum 2 instrument with the resolution 4 cm<sup>-1</sup>. To investigate the nature of the acid sites, liquid pyridine was absorbed onto Cs<sub>0.7</sub>TO and Cs<sub>0.7</sub>ZnTO in a closed vial, followed by drying at 50 °C overnight prior to acquiring the spectrum in ATR mode. Raman spectra were recorded using a DXR Smart Raman (Thermoscientific) at the laser wavelength of 532 nm and the laser power of 5 mW.

#### 3.3) Temperature-programmed desorption

For NH<sub>3</sub> TPD, ~0.2 g of the sample was loaded into the center of a quartz tube reactor and covered with quartz wool. The sample was activated at  $T_a = 300$ , 400 or 500 °C for 2 h, cooled down to ~30 °C (both under flowing air of 10 °C·min<sup>-1</sup>), followed by the adsorption of 1% NH<sub>3</sub>/He (50 mL·min<sup>-1</sup>) for 1 h. Then, physisorbed NH<sub>3</sub> was purged with helium (30 mL·min<sup>-1</sup>) until the baseline as detected by the thermal conductivity detector was flat, commonly for an hour. The profile was next collected from 50 to 700 °C (10 °C·min<sup>-1</sup>) under a flow of helium.

The acidity is expressed as  $\mu$ mol NH<sub>3</sub>·g<sup>-1</sup> of the solid which was quantified by comparison to H-ZSM-5 (PZ-2/1000H, Zeochem; nominal Si/Al = 500). Considering the experimental (by XRF) Si/Al of 422 and the general chemical composition H<sub>n</sub>Al<sub>n</sub>Si<sub>96</sub>.  $_{n}O_{192}$ ·H<sub>2</sub>O, the value n = 0.227 was obtained, giving the formula weight of the zeolite 5786.07 g·mol<sup>-1</sup>. So, the theoretical acidity equals  $(0.227 \times 10^6/5786.07)$  or 39.2  $\mu$ mol·g<sup>-1</sup>. From the peak area at the NH<sub>3</sub> desorption temperature >400 °C characteristics of the Brønsted sites, the acidity of 33.2  $\mu$ mol·g<sup>-1</sup> was obtained. This result indicates a reasonable agreement in experimental  $\nu$ s theoretical acidity, with the difference of (39.2-33.2)×100%/39.2, or ~15%, which will not affect the discussion. In addition, the theoretical acidity of 39.2  $\mu$ mol·g<sup>-1</sup> is in excellent agreement with 40.3  $\mu$ mol·g<sup>-1</sup> determined in a separate isopropylamine (IPA)-TPD experiment (later).

The isopropylamine (IPA)-TPD, which is specific to Brønsted acid sites  $^{44,45}$  only, was performed as follows. An aliquot of 1  $\mu$ L of IPA was repeatedly injected at RT, onto 0.1 g of Cs<sub>0.7</sub>TO (activated at 400 °C under air) as a representative sample under the flow of He (30 mL/min). The total amount of injected IPA was 10  $\mu$ L. Then, the purging

and temperature-programmed desorption was conducted as described above for NH<sub>3</sub> TPD. Propylene, which is the decomposition product of IPA over Brønsted acid sites, was detected by a flame ionization detector. Similar experiment was performed with H-ZSM-5.

The temperature-programmed desorption of  $CO_2$  ( $CO_2$  TPD) measurements were performed similar to the NH<sub>3</sub> TPD, but with the single  $T_a$  = 450 °C for 2 h and under N<sub>2</sub>.  $CO_2$  gas (99.99%) was then fed to the sample at a flow rate 30 mL·min<sup>-1</sup> for an hour, followed by flushing with He (30 mL·min<sup>-1</sup>, 1 h). The temperature was then raised from 50 °C to 600 °C (5 °C·min<sup>-1</sup>) under He. Basicity is expressed as  $\mu$ mol  $CO_2 \cdot g^{-1}$  which was quantified by comparison with a known mass of calcium oxalate which convert to  $CO_2$  stoichiometrically.

#### 3.4) Catalytic activity testing

The catalyst (pressed and sieved to the fraction 600-850  $\mu$ m) was packed into a vertical glass tube reactor, and covered with glass wool and glass bead. Prior to activity testing, it was heated from RT to 400 °C (10 °C min<sup>-1</sup>), hold for 2 h, and cool down to 380 °C (all under flowing air, 30 mL·min<sup>-1</sup>). Then, 99.99% absolute ethanol (Carlo Erba) was fed into the reactor by a syringe pump at 1 mL·h<sup>-1</sup>. N<sub>2</sub> was used as a carrier gas at 60 mL·min<sup>-1</sup>, corresponding to the contact time (*WIF*) of 58 g·h·mol<sup>-1</sup>. The catalytic testing was conducted for a total time on stream of 6 h. The products were periodically analyzed using an online BUCK Scientific 910 gas chromatograph (GC) equipped with the FID and the FFAP column (30m×0.25mm×0.25 $\mu$ m), by comparison with the retention time and peak area of the standard of known concentration.

#### 4. Results and Discussion

#### 4.1) Structural characteristics

All cesium titanate samples are white, plate-like microcrystals with the particle size of ~0.5  $\mu$ m as shown on the right of Figure 1 for Cs<sub>0.7</sub>TO as a representative. Figure 2 shows the XRD patterns of the investigated samples which are all characteristics of the lepidocrocite-type cesium titanate (*Immm*). The 011 reflection (x in Figure 2) typically overlaps with the 060 reflection in the  $\square$ -containing sample Cs<sub>x</sub>TO (x = 0.70, 0.67), which is in agreement with the report by Grey *et al.* Upon substituting Zn for Ti in the Cs<sub>0.7</sub>ZnTO, these two peaks are clearly separated; this finding is also consistent with the calculated XRD pattern by Gao *et al.* Table 1 lists the corresponding unit cell parameters, which agree reasonably with reported 1.31,33,46,47 values. (The differences might be due to small variations in stoichiometry from different laboratories.) Taking Cs<sub>0.7</sub>TO as an example, the unit cell parameters as determined by CellCalc 48 are: a = 3.815(4), b = 17.46(2) and c = 2.961(6) Å, with the interlayer spacing  $d_{0.20}$  (= b/2) ~8.6 Å. This distance in Cs<sub>0.7</sub>TO is larger than 7.8 Å in the potassium analog K<sub>0.8</sub>ZnTO, 32,34,5 but is smaller than 9.4 Å in the related structure *e.g.*, Cs<sub>2</sub>Ti<sub>5</sub>O<sub>11</sub>.

12

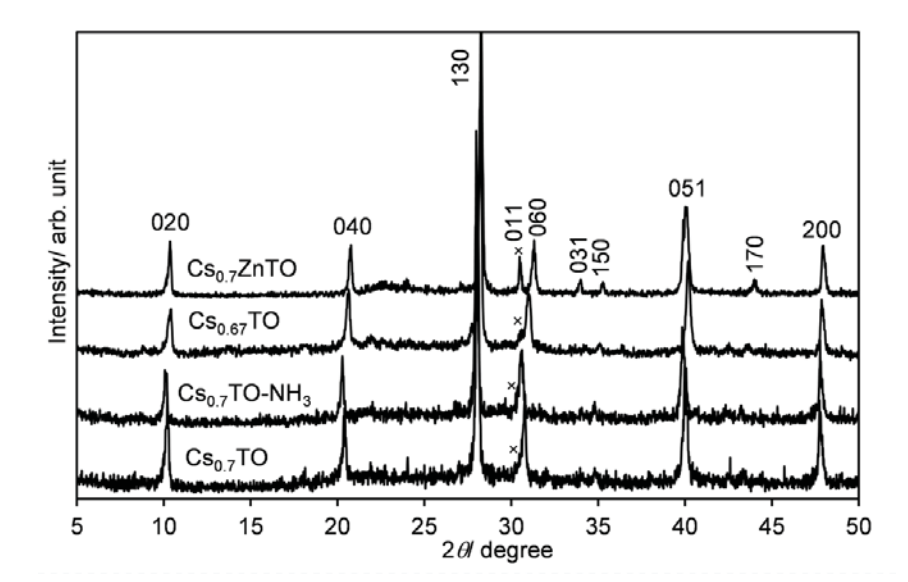


Figure 2. XRD patterns of the cesium titanate samples investigated in this work, including the respective hkl indexes shown atop the peak. Crossmark (×) is the 011 reflection which overlap or separate from the nearby 060 reflection, depending on the composition. <sup>14,33</sup>

Table 1. Unit cell parameters of the samples.

Sample	a/ Å	b/ Å	c/ Å	Ref.
$Cs_{0.7}TO (Cs_{0.7}Ti_{1.825}\square_{0.175}O_4)$	3.815(4)	17.46(2)	2.961(6)	This work
	3.837(1)	17.198(3)	2.960(1)	31
Cs <sub>0.7</sub> TO-NH <sub>3</sub> (Cs <sub>0.7</sub> TO after NH <sub>3</sub>	3.819(5)	17.54(5)	2.957(3)	This work
TPD) $Cs_{0.67}TO (Cs_{0.67}Ti_{1.8325}\square_{0.1675}O_4)$	3.803(4)	17.38(2)	2.939(7)	This work
	3.823	17.215	2.955	46,47
$Cs_{0.7}Zn_{0.35}TO (Cs_{0.7}Zn_{0.35}Ti_{1.65}O_4)$	3.7949(8)	17.12(6)	2.974(1)	This work
	3.8143(1)	17.0205(4)	2.9837(1)	33
K <sub>0.8</sub> ZnTO (K <sub>0.8</sub> Zn <sub>0.4</sub> Ti <sub>1.6</sub> O <sub>4</sub> )	3.809(3)	15.67(1)	2.981(2)	5,6
$H_{0.7}TO (H_{0.70}Ti_{1.825}\square_{0.175}O_4\cdot H_2O)$	3.790(3)	18.43(3)	2.953(5)	This work
	3.783(2)	18.735(8)	2.978(2)	31

#### 4.2) Thermal stability

Figure 2 also compares the XRD patterns of  $Cs_{0.7}TO$  vs  $Cs_{0.7}TO$ -NH<sub>3</sub> (*i.e.*, after the NH<sub>3</sub> TPD measurement where the temperature up to 700 °C was reached). Importantly, the similarity in these two patterns suggests the preservation of the lepidocrocite-type structure. The unit cell parameters between the two are also similar, Table 1. Using the full width at half maximum of the 020 peak and the Scherrer equation, an almost identical crystallite size D was obtained (42 nm for  $Cs_{0.7}TO$ ; 38 nm for  $Cs_{0.7}TO$ -NH<sub>3</sub>), also indicating minimal structural changes.

In addition, the Raman spectra of the two samples shown in Figure 3a are generally similar and show bands characteristics <sup>10,13</sup> of the lepidocrocite-type cesium titanate. These bands are typically assigned to the stretching vibration of the Ti-O of the layers. <sup>10,13</sup> In particular, the preservation of the peak at 914-917 cm<sup>-1</sup> due to Cs-O stretching <sup>10,13</sup> suggests that Cs<sup>+</sup> ions persist in a similar local environment, either prior to or after the NH<sub>3</sub> TPD measurement.

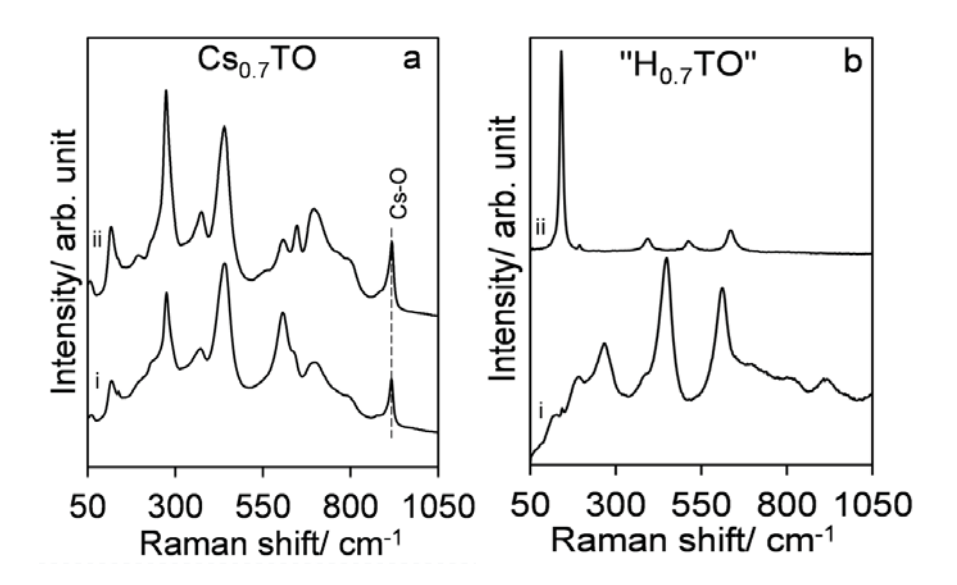


Figure 3. Raman spectra of (a)  $Cs_{0.7}TO$  and (b)  $H_{0.7}TO$ , either (i) prior to or (ii) after the  $NH_3$  TPD measurement where the temperature up to 700 °C was reached.

For comparison, the protonic form  $H_{0.7}TO$  (*i.e.*,  $H_{0.70}Ti_{1.825}\Box_{0.175}O_4\cdot H_2O$ ) was prepared via repeated equilibration of  $Cs_{0.7}TO$  with HCI. The XRD pattern of  $H_{0.7}TO$  and the corresponding unit cell parameters shown in Figure 4a and Table 1, respectively, agree with the literature. This material with the expanded interlayer separation ( $d_{020} = b/2 \sim 9.2$  Å) contains the interlayer Brønsted acid sites and the water molecule. However, after the NH3 TPD measurement, the characteristic Raman vibrations of the protonic lepidocrocite ( $H_{0.7}TO$ ) was completely disappeared as shown in Figure 3b. Instead several peaks indicative of anatase-type  $TiO_2^{52}$  are visible, confirming the lepidocrocite-to-anatase transformation.

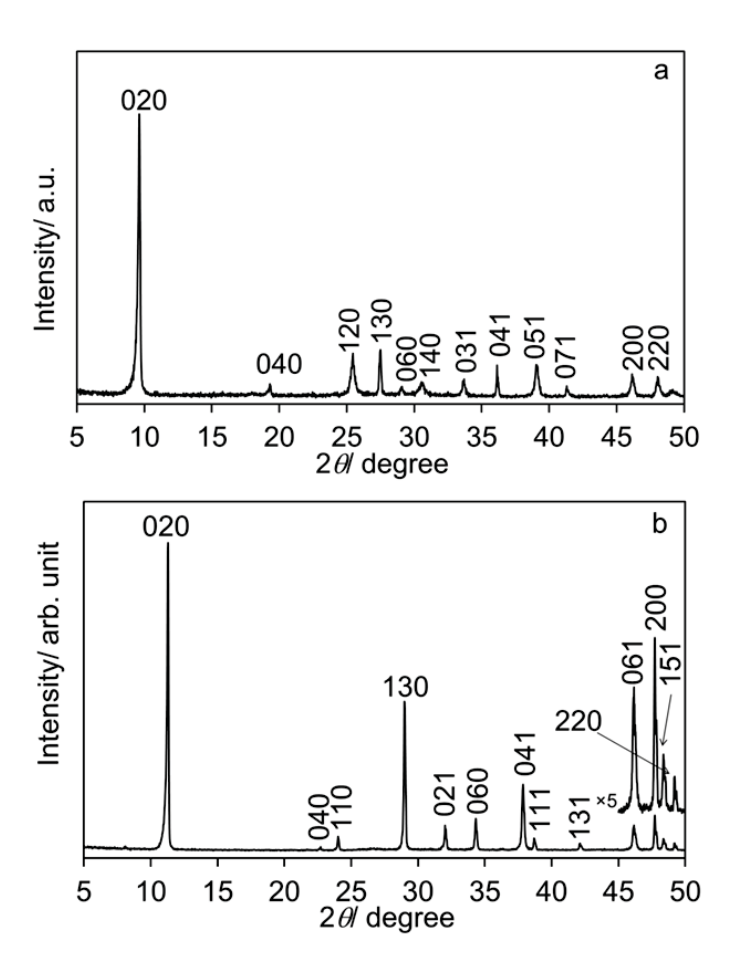


Figure 4. XRD patterns of (a)  $H_{0.7}TO$ , and (b)  $K_{0.8}ZnTO$ .

Such limited thermal stability of  $H_{0.7}TO$  can also be deduced from the massive mass loss (~15 wt%, Figure 5) upon heating to 700 °C under  $N_2$  in a separate thermogravimetric analysis. This mass loss has been ascribed to dehydration and dehydroxylation, accompanied by the subsequent collapse of the lepidocrocite-type layers and the condensation to anatase. On the other hand, the tested compositions of the cesium titanate show a limited loss (~2.5-5.0 wt%), ascribed to the liberation of water on the external surfaces. Altogether, these results highlight the superior thermal stability of the cesium analog with respect to the protonic form.

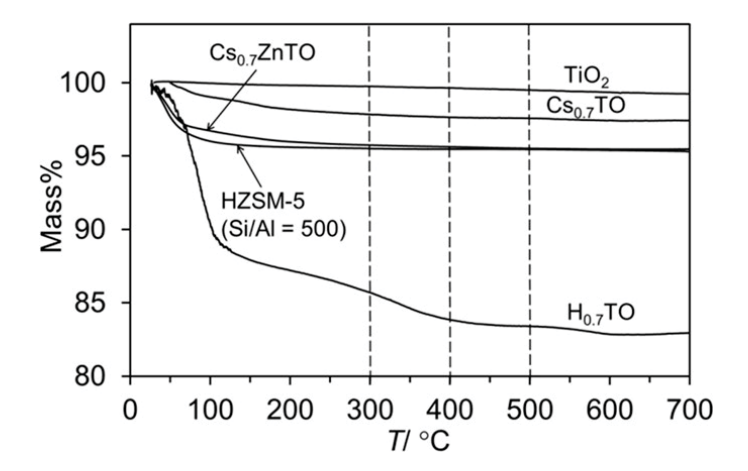


Figure 5. The mass loss curve of several samples recorded under  $N_2$ . The dash bar at 300-500 °C indicates the activation temperature  $T_a$  where the NH $_3$  TPD measurements were carried out.

#### 4.3) Acid strength and acidity

The acid strength and acidity of the titanate was first investigated by NH $_3$  TPD after activation of the samples at 400 °C, where the contribution from surface water can be excluded (Figure 5). The variation in maximum peak temperature  $T_m$  was within 10 °C, while the accuracy in acidity was ~15%.

As shown in Figure 6, the  $Cs_{0.7}TO$  with Ti vacancy  $\square$  desorbs  $NH_3$  in two ranges at 100-300 °C (low-temperature, LT) and above 400 °C (high temperature, HT). The respective  $T_m$  is at ~145, 470 °C. Similar behavior was observed in other compositions tested but with a higher  $T_m$ , including  $Cs_{0.67}TO$  (also with  $\square$ ) and  $Cs_{0.7}ZnTO$  (where the  $\square$  sites were filled with Zn, later). While it is well known that  $T_m$  is sensitive to several parameters, the  $NH_3$  desorption from the cesium titanate samples at >400 °C strongly suggests the presence of strong acid sites. The increased acidic strength of  $Cs_{0.7}ZnTO$  (*i.e.*, a higher  $T_m$  especially at the HT-range) might be explained by the electron withdrawing effect of Zn, as inferred from Sanderson's electronegativity  $^{56,57}$  (2.223 for Zn, 1.50 for Ti). Considering that the intercalated  $NH_3$  in  $M^{2+}$ -exchanged  $H_{0.7}TO$  was earlier released at <300 °C,  $^{36}$  our results demonstrate the remarkable acidic nature in the cesium titanate.

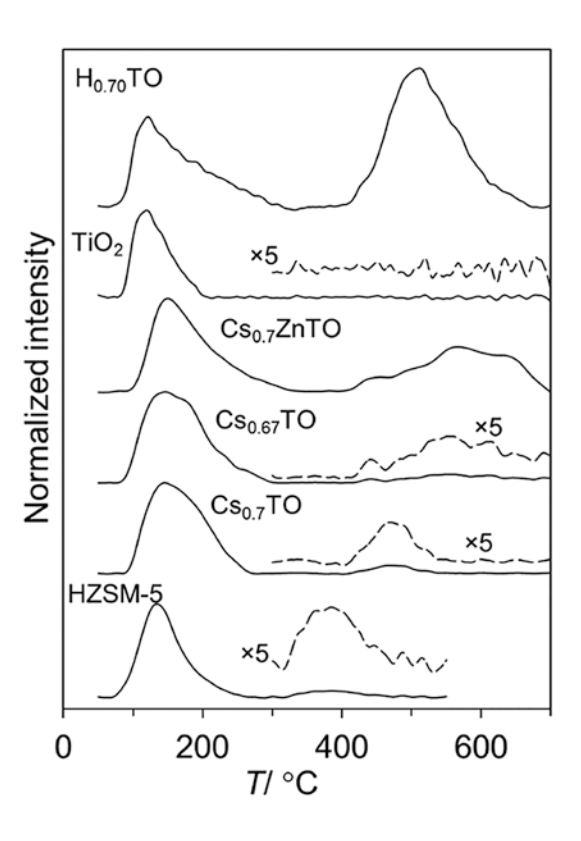


Figure 6.  $NH_3$  TPD profiles from the samples activated at 400 °C. The profiles were normalized so that the LT-peak is of the same height. Dash lines at HT-range were magnified by a factor of 5.

The acidic strength of these cesium titanates appears to be higher than that observed in relevant samples. It was found that anatase-type  $TiO_2$  desorbs  $NH_3$  only at the LT ( $T_m \sim 130$  °C) without any HT peak. Even for HZSM-5 (Si/AI = 500), its LT- and HT-desorption occur at the temperature slightly lower than that from the cesium titanate samples. For the protonic  $H_{0.7}TO$  with Brønsted acid sites, the layer collapse and structural transformation<sup>31</sup> as described above certainly contributes to the desorption profile, including that reported<sup>58</sup> previously. So, the acidic nature of  $H_{0.7}TO$  will not be discussed further.

Table 2 summarizes the total acidity, which is a combination of LT- and HT-acidity. At the activation temperature of 400 °C, the acidity of  $Cs_{0.7}TO$  (~280  $\mu$ mol g<sup>-1</sup>) is ~5 times larger than that of  $TiO_2$  with similar  $S_{BET}$ . The low specific surface area  $S_{BET}$  (here ~5-6 m<sup>2</sup> g<sup>-1</sup>) is rather common for the samples prepared via a traditional, high-temperature solid state synthesis with the micron-sized  $TiO_2$  as the reactant. It indicates that the microcrystals are essentially regarded as non-porous materials, and that the  $N_2$  adsorption/desorption would mostly occur at the external surfaces. Therefore, the large acidity observed for  $Cs_{0.7}TO$  despite of a low  $S_{BET}$  suggests the NH<sub>3</sub> adsorption at the internal surfaces (*i.e.*, intercalation), requiring *in situ* XRD for further characterizations.

Table 2. Summary of specific surface area  $S_{\it BET}$ , acidity at low- and high-temperature (LT and HT), including the maximum peak temperature  $T_{\it m}$ , and the total acidity as determined by NH $_3$  TPD.

Entry	Sample <sup>a</sup>	S <sub>BET</sub> /	LT acidity/	HT acidity/	Total acidity/
1a	Cs <sub>0.7</sub> TO-300	5	347 (143)	64 (418)	410
1b	Cs <sub>0.7</sub> TO-400	5	264 (145)	15 (470)	279
1c	Cs <sub>0.7</sub> TO-500	5	252 (133)	Not detected	252
2	Cs <sub>0.67</sub> TO-400	15	397 (152)	60 (557)	458
3a	Cs <sub>0.7</sub> ZnTO-300	6	100 (139)	108 (421)	206
3b	Cs <sub>0.7</sub> ZnTO-400	6	74 (148)	61 (566)	135
3c	Cs <sub>0.7</sub> ZnTO-500	6	66 (145)	6 (586)	72
4	K <sub>0.8</sub> ZnTO-400	3	N.D.	N.D.	N.D.
5a	TiO <sub>2</sub> -400	6	60 (126)	N.D.	60
5b	TiO <sub>2</sub> -700	6	56 (132)	N.D.	56
6	H <sub>0.7</sub> TO-400	N.A.	133 (121)	178 (512)	311
7	HZSM-5-400	350	361 (150)	30 (400)	392

 $^a$ Cs<sub>x</sub>TO (Cs<sub>x</sub>Ti<sub>2-x/4</sub> $\square_{x/4}$ O<sub>4</sub>; x = 0.67, 0.70), Cs<sub>0.7</sub>ZnTO (Cs<sub>0.7</sub>Zn<sub>0.35</sub>Ti<sub>1.65</sub>O<sub>4</sub>), K<sub>0.8</sub>ZnTO (K<sub>0.8</sub>Zn<sub>0.4</sub>Ti<sub>1.6</sub>O<sub>4</sub>), and H<sub>0.7</sub>TO (H<sub>0.7</sub>Ti<sub>1.825</sub> $\square_{0.175}$ O<sub>4</sub>·H<sub>2</sub>O). The number after the name indicates the activation temperature  $T_a$  (in °C) prior to NH<sub>3</sub> adsorption. N.A. = not available; N.D. = not detected.

It is also found that acidity of the  $\Box$ -containing Cs<sub>0.7</sub>TO is increased with the decrease in the activation temperature  $T_a$ , reaching ~410  $\mu$ mol g<sup>-1</sup> at  $T_a$  = 300 °C as summarized in Table 2 (Entry 1a-c). This behavior is in sharp contrast to TiO<sub>2</sub> exhibiting relatively constant (but low) acidity at  $T_a$  = 400, 700 °C (Entry 5a,b). (The acidity of TiO<sub>2</sub> reported here is within the literature values, Table 3). Different HT-desorption pattern for Cs<sub>0.7</sub>TO activated at different temperature (Figure 7a), suggests a complex alteration of surface functionals (e.g., Ti vacancy  $\Box$ ) or surface re-arrangement. <sup>34,59,60</sup> In-situ surface analyses will be required to test these hypotheses. The acidity increased in part with the increase in  $S_{BET}$ , as demonstrated for Cs<sub>0.67</sub>TO prepared from the nanosized <sup>42</sup> P25 TiO<sub>2</sub> (Table 2, Entry 2).

Table 3. Selected examples on  $T_m$  and acidity of TiO<sub>2</sub> and protonic/alkali titanate.<sup>a</sup>

Sample	S <sub>BE7</sub> / m <sup>2</sup> ·g <sup>-1</sup>	J., /L	Acidity/ µmol·g	Analytical method	Ref.
Lepidocrocite-type Cs <sub>0.7</sub> Ti <sub>1.825</sub> O <sub>4</sub>	5		252-410	NH <sub>3</sub> TPD	This work
Lepidocrocite-type Cs <sub>0.67</sub> Ti <sub>1.8325</sub> O <sub>4</sub>	15		458	NH <sub>3</sub> TPD	This work
Lepidocrocite-type Cs <sub>0.7</sub> Zn <sub>0.35</sub> Ti <sub>1.65</sub> O <sub>4</sub>	9		72-206	NH <sub>3</sub> TPD	This work
TiO <sub>2</sub>	54	169	297	NH <sub>3</sub> TPD	61
TiO <sub>2</sub>	110	310	173	NH <sub>3</sub> TPD	62
TiO <sub>2</sub>	300	Not applicable	130	Pyridine FTIR	27
TiO <sub>2</sub> P25 (Degussa)	48	55, 143, 250	8.5	NH <sub>3</sub> TPD	63
TiO <sub>2</sub> P25 (Degussa)	52	Not reported	15.2	NH <sub>3</sub> TPD	64
TiO <sub>2</sub> (Hombikat)	204	Not reported	23.2	NH <sub>3</sub> TPD	64
TiO <sub>2</sub> (Aldrich)	41	Not reported	1.1	NH <sub>3</sub> TPD	64
TiO <sub>2</sub> (Kemira)	50	Not reported	11.0	NH <sub>3</sub> TPD	64

Table 3. continued

Sample	$S_{BE7}/ \text{ m} \cdot \text{g}^{-1}$	J., /"L	Acidity/ µmol·g	Analytical method	Ref.
TiO <sub>2</sub> nanosheets	420	Not applicable	086	TH NMR	25
Na <sub>2</sub> Ti <sub>3</sub> O <sub>7</sub> nanotubes	135	150	300	NH <sub>3</sub> TPD	65
H <sub>2</sub> Ti <sub>3</sub> O <sub>7</sub> microcrystals	56	150, 350	100	NH <sub>3</sub> TPD	65
H <sub>2</sub> Ti <sub>3</sub> O <sub>7</sub> nanotubes	182-313	<100	240-330	Pyridine TPD/ TG analysis	30
H₂Ti₃O <sub>7</sub> nanowires	35	207,504	Not reported	NH <sub>3</sub> TPD	99
H <sub>2</sub> Ti <sub>3</sub> O <sub>7</sub> nanotubes	350	290	1,100	NH <sub>3</sub> TPD	65
H <sub>2</sub> Ti <sub>3</sub> O <sub>7</sub> nanotubes	305	Not applicable	470	Pyridine FTIR	37
H <sub>2</sub> Ti <sub>3</sub> O <sub>7</sub> nanotubes	286	161, 302	3,775	NH <sub>3</sub> TPD	29
H <sub>2</sub> Ti <sub>3</sub> O <sub>7</sub> nanotubes	400	Not reported	350	Pyridine FTIR	26 27 28
H <sub>2</sub> Ti <sub>3</sub> O <sub>7</sub> nanosheets	75	Not reported	150	Pyridine FTIR	26 27

Table 3. continued

Sample	S <sub>BET</sub> / m <sup>2</sup> ·g	J., "L	Acidity/ µmol·g	Analytical method	Ref.
H₂Ti₄O <sub>9</sub> ·H₂O nanotubes	325	Not reported	340	Pyridine FTIR	89
H <sub>0.7</sub> TO	16	Not reported	20	Pyridine FTIR	26 27
$H_{0.7}TO$ pillared with $n$ -butylamine/SiO $_2$	27	Not applicable	200	Cyclohexylamine adsorp.	23
$H_{0.7}TO$ pillared with <i>n</i> -hexylamine/SiO $_2$	62	Not applicable	500	Cyclohexylamine adsorp.	23
$H_{0.7}TO$ pillared with <i>n</i> -nonylamine/SiO $_2$	102	Not applicable	760	Cyclohexylamine adsorp.	23
H <sub>0.7</sub> TO nanosheets	106	Not reported	210	Pyridine FTIR	26 27
H <sub>1.4</sub> Tī <sub>1.65</sub> O <sub>4</sub> ·H <sub>2</sub> O nanosheets	183	98, 250	Not reported	NH <sub>3</sub> TPD	28
(H <sub>3</sub> O) <sub>0.5</sub> H <sub>1.5</sub> Ti <sub>8</sub> O <sub>17</sub> ·H <sub>2</sub> O	100	Not applicable	1,100	NH <sub>3</sub> microcalorim. adsorption	69

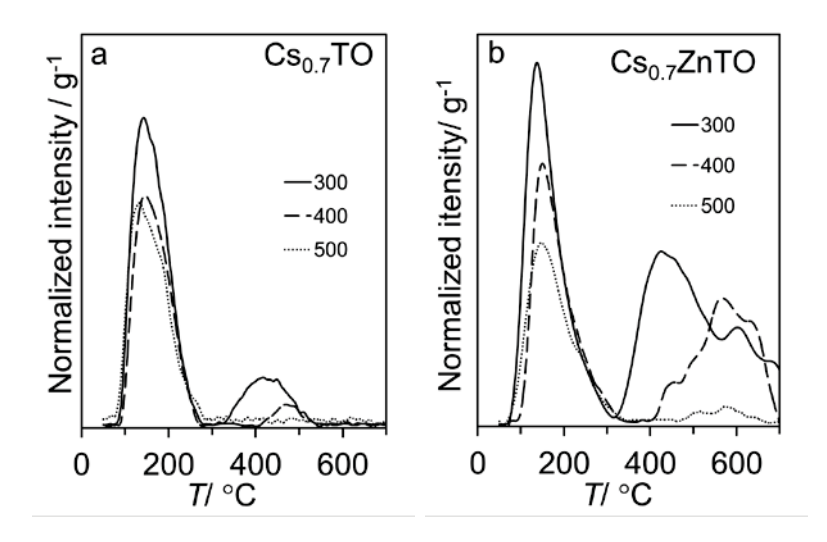


Figure 7. Temperature profiles of NH<sub>3</sub> desorption of from (a) Cs<sub>0.7</sub>TO, and (b) Cs<sub>0.7</sub>ZnTO activated at  $T_a$  = 300, 400, and 500 °C. Each profile was normalized by the mass of the sample.

When the Ti vacancy sites ( $\square$ ) were filled by Zn,<sup>33</sup> the total acidity of Cs<sub>0.7</sub>ZnTO is reduced to half that of Cs<sub>0.7</sub>TO at similar  $S_{BET}$  (Table 2). For example at the activation temperatures  $T_a = 300$  °C, the LT acidity/HT acidity is  $100/108 \ \mu \text{mol} \cdot \text{g}^{-1}$  for Cs<sub>0.7</sub>ZnTO, but it is  $347/64 \ \mu \text{mol} \cdot \text{g}^{-1}$  for Cs<sub>0.7</sub>TO. This behavior was observed at all  $T_a$  studied as also shown in Figure 7b and in Table 2 (Entry 3a-c). In fact, the drop in total acidity upon Zn substitution is due to a *notable decrease* in LT-acidity, which is accompanied by the *moderate increase* in HT-acidity. This result suggests that Ti atoms at the proximity of the vacancy sites could be specifically responsible for NH<sub>3</sub> LT-desorption. (The formation of hydroxylated groups due to water adsorption around the  $\square$  sites is energetically favorable;  $^{70,71}$  however the adsorption of NH<sub>3</sub> has not been reported to the best of our knowledge.) Importantly, the observed acidity increase at the

HT-desorption in  $Cs_{0.7}ZnTO$  indicates the presence of another sort of acid sites, which are not associated with the  $\square$  sites (see also XPS results, below).

The acidic nature of the cesium titanate microcrystals reported here suggests novel bifunctional property of these materials, since only the basic nature of the lattice oxygen has been reported  $^{5,6}$  so far for lepidocrocite-type  $K_xM_yTi_{2-y}O_4$ . The  $CO_2$  TPD measurements were performed and the results are summarized in Figure 8 and Table 4.

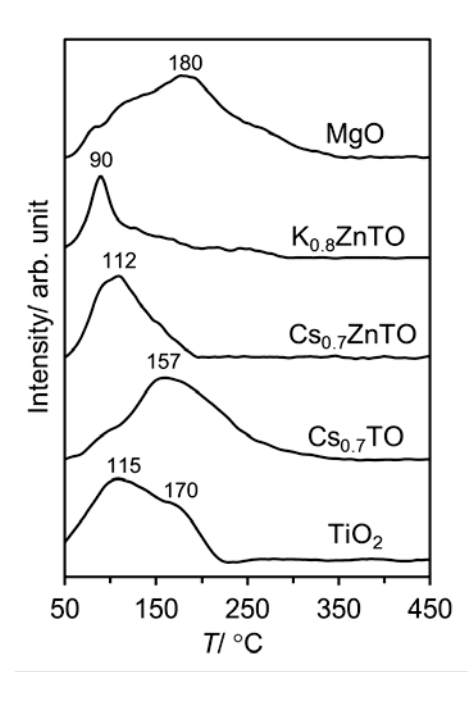


Figure 8. Temperature profiles of  $CO_2$  desorption from selected samples. Data for MgO and  $K_{0.8}$ ZnTO are from the previous work. The desorption from MgO at 450-650 °C due to the decomposition of bulk MgCO<sub>3</sub> produced *in situ* is not shown. There are no desorption peaks in this range for other samples.)

Table 4. Summary of the CO<sub>2</sub> TPD results.

Sample	$S_{BET}/ \text{ m}^2 \cdot \text{g}^{-1}$	T <sub>m</sub> / °C	Basicity/ <i>μ</i> mol·g <sup>-1</sup>
TiO <sub>2</sub>	6	115	68
$Cs_{0.7}TO (Cs_{0.70}Ti_{1.825}\square_{0.175}O_4)$	5	157	175
$Cs_{0.7}ZnTO (Cs_{0.70}Ti_{1.825}\square_{0.175}O_4)$	6	112	47
K <sub>0.8</sub> ZnTO <sup>5,6</sup>	3	90	39
MgO	63	180	314

<sup>&</sup>lt;sup>a</sup> from N<sub>2</sub> adsorption isotherm

Although  $Cs_{0.7}TO$  exhibits typical basicity, the ratio of (desorbed  $NH_3$ )/(desorbed  $CO_2$ ) which approximately represents the contribution of acid-to-basic sites is 1.6. This ratio as determined in a similar manner from  $Cs_{0.7}ZnO$  is 2.9. Clearly, these numbers are significantly higher than  $TiO_2$  (0.9). Again, this result emphasizes the unusually acidic nature of the lepidocrocite-type cesium titanate, contrasting the basic site-dominating surfaces in other titanates such as the  $ATiO_3$  (A = Sr, Ba) perovskite.

The essential influence of polarizable  $Cs^{+}$  ions toward the acidic properties is further emphasized by comparing the  $\square$ -free but Zn-containing  $Cs_{0.7}ZnTO$  ( $Cs_{0.7}Zn_{0.35}Ti_{1.65}O_4$ , space group Immm,  $^{33}S_{BET}=6$  m $^2\cdot g^{-1}$ ) to  $K_{0.8}ZnTO$  ( $K_{0.8}Zn_{0.4}Ti_{1.6}O_4$ , space group  $Cm2c_1$ ,  $^{32}S_{BET}=3$  m $^2\cdot g^{-1}$ , Figure 4b). It was found out that, while  $Cs_{0.7}ZnTO$  shows considerable NH<sub>3</sub> adsorption/desorption, the NH<sub>3</sub> adsorption/desorption from  $K_{0.8}ZnTO$  was completely diminished resulting in a flat TPD

profile (not shown). This point will be discussed below regarding the nature of the acid sites.

Altogether, while the  $S_{\it BET}$  of the cesium titanate is rather low and has not yet been optimized, their acidity is comparable to that of typical acid zeolites  $^{43,73,74}$  or some high-acidity protonic titanate samples with much larger  $S_{\it BET}$  (Table 3). This is rather exceptional since the samples are in the form of microcrystals—without the need for lengthy protonation/ion exchange, pillaring, delamination or restacking—and virtually have no porosity.

#### 4.4) Possible nature of acid sites

Figure 9a shows the IR spectra of pyridine-sorbed Cs<sub>0.7</sub>TO and Cs<sub>0.7</sub>ZnTO. The strong peak at ~1440 cm<sup>-1</sup> typical of pyridine bound to Lewis acid sites<sup>28,75</sup> is clearly observed. On the contrary, the signal characteristics of pyridine bound to Brønsted acid sites is absent in these two samples. For K<sub>0.8</sub>ZnTO, only vibrations due to the titanate itself was observed but without any signal due to sorbed-pyridine (not shown). This result is in good agreement with the flat NH<sub>3</sub> TPD profile mentioned previously. In addition, the TPD experiment with isopropylamine which is specific to Brønsted acid sites<sup>44,45</sup> also showed virtually zero adsorption/desorption (not shown). Accordingly one can deduce that Cs<sub>0.7</sub>TO and Cs<sub>0.7</sub>ZnTO are the Lewis acid as anticipated. Since the interlayer Cs<sup>+</sup> ions cannot be the Lewis acid center, it is most likely that the Ti<sup>4+</sup>,M<sup>n+</sup> ions on the accessible surfaces of the sheets (*i.e.* basal plane or edges) are the acid sites.

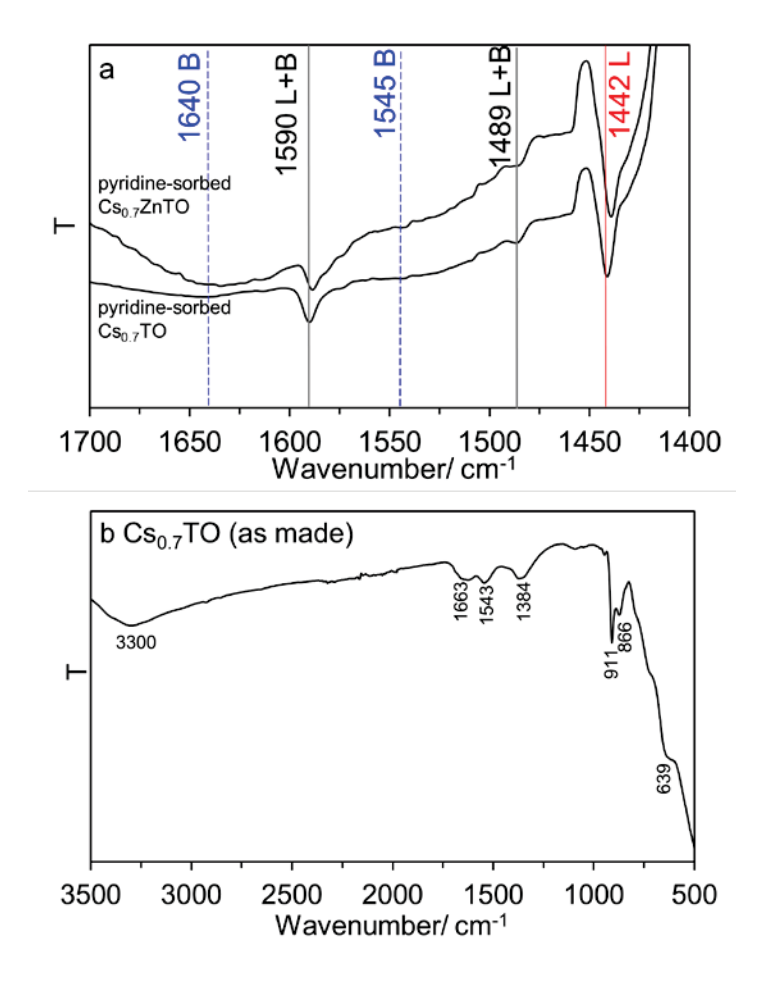


Figure 9. (a) ATR spectra of pyridine-sorbed  $Cs_{0.7}TO$  and  $Cs_{0.7}ZnTO$  with the vibrations characteristics of pyridine adsorbed on Lewis (L), Brønsted (B), or the combination of these two sites (L+B) indicated; (b) the ATR spectrum of  $Cs_{0.70}TO$ .

In line with this view, the sorption of atmospheric water by  $Cs_{0.7}TO$  microcrystals (the ~2.5wt% water, Figure 5), despite of small  $S_{BET}$  and essentially no porosity, suggests the interaction between the electron-rich oxygen atom in water molecules (*i.e.*, the Lewis base) and the under-coordinated, electron-poor  $Ti^{4+}$  ions on the surfaces (*i.e.*, the Lewis acid). The acidic  $Cs_{0.7}ZnTO$  also showed a mass loss due to water sorption of ~5 wt% despite of a similar  $S_{BET}$  to  $Cs_{0.7}TO$ . The presence of surface hydroxyls, arising

from adsorbed water,<sup>5</sup> can also be inferred from the stretching/bending vibration at ~3300/1660 cm<sup>-1</sup> shown in Figure 9b. The hydroxyl group attached to the layers<sup>5</sup> was found at 911 cm<sup>-1</sup>. Small peaks at 1384 and 1543 cm<sup>-1</sup> are due to vibrations from surface carbonate or bicarbonates.<sup>5</sup> Lastly, the lattice vibration of  $TiO_6$  octahedra<sup>5</sup> appears at 639 and 866 cm<sup>-1</sup>. However, the attempt to detect the surface Ti species by diffuse reflectance ultraviolet-visible (DRUV) spectroscopy was unsuccessful, likely due to the low  $S_{BET}$  of the samples and consequently the small amount of such species. A careful surface-sensitive analysis will be further required, which will provide not only the information on the local structure, but also the possible correlation (if any) with catalytic activities in the future contribution.

Accordingly, the Ti2p XPS spectra of some samples were recorded and compared in Figure 10. Note that the Ti2p signals are the average of all surface Ti species probed (analysis area  $300 \times 300 \ \mu\text{m}^2$ ), including Ti at the proximity of  $\Box$  (and Zn), and Ti that is away from it. In all cases the binding energy indicates the presence of Ti<sup>4+</sup> as anticipated. <sup>33,34,58,76,77</sup> Specifically, the  $\Box$ -containing Cs<sub>0.7</sub>TO shows the peaks at 459.3 eV (Ti2p<sub>3/2</sub>) and 465.0 eV (Ti2p<sub>1/2</sub>) which are more positive by ~1 eV than the corresponding signals in TiO<sub>2</sub> (458.4 and 464.1 eV). In the Zn-substituted Cs<sub>0.7</sub>ZnTO, the Ti2p signals at similar binding energies (459.3, 465.1 eV) to Cs<sub>0.7</sub>TO were observed. (The presence of another component at 457.8, 463.5 eV might as well suggest another sort of acid sites.) Such electropositive nature of surface Ti atoms in Cs<sub>0.7</sub>TO and Cs<sub>0.7</sub>ZnTO in relation to TiO<sub>2</sub> agrees qualitatively with the results from NH<sub>3</sub> TPD (Figure 6). For K<sub>0.8</sub>ZnTO, <sup>34</sup> the majority of the Ti2p peak (458.1 eV, Ti2p<sub>3/2</sub>; and 463.8 eV, Ti2p<sub>1/2</sub>) is close to that in TiO<sub>2</sub>. Clearly, the surface Ti species in K<sub>0.8</sub>ZnTO are not as

electropositive as that in  $Cs_{0.7}TO$  and  $Cs_{0.7}ZnTO$ . It is worth noting that  $Cs_{0.7}TO$  with 0.7 positive-charge per formula unit (x) is more acidic than the potassium analog with 0.8 positive-charge per formula unit. So, the interlayer cation seems to have a stronger effect toward acidic character. A better understanding might be obtained by studying the compositions with mixed interlayer alkali ions (i.e.,  $Cs_{0.7-x}K_xZn_{0.35}Ti_{1.65}O_4$  vs  $Cs_{0.7}Zn_{0.35}Ti_{1.65}O_4$ ).

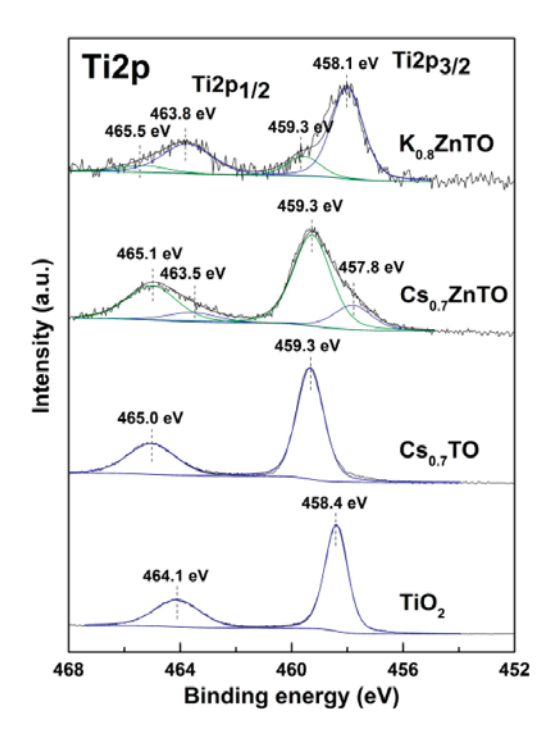


Figure 10. Ti2p XPS spectra of anatase-type  $TiO_2$ ,  $Cs_{0.7}TO$ ,  $Cs_{0.7}ZnTO$  and  $K_{0.8}ZnTO$ .

The relative distribution of  $Ti^{4+}$  might be indirectly inferred from the compositional analyses of the  $Cs_{0.7}TO$  microcrystals (i.e.,  $Cs_{0.7}Ti_{1.825}\square_{0.175}O_4$ ) where the nominal Ti/Cs equals 2.60. The surface Ti/Cs (as determined by XPS) was  $4.1\pm0.5$ , larger than that in the bulk ( $2.94\pm0.02$  for XRF,  $2.9\pm0.2$  for EDX). That is, Ti-termination and/or surface Ti enrichment was observed in  $Cs_{0.7}TO$ , potentially rendering the acidic

character. For  $Cs_{0.7}ZnTO$  ( $Cs_{0.7}Zn_{0.35}Ti_{1.65}O_4$ ), the (Ti+Zn)/Cs ratios obtained from different techniques were similar: 2.86 (nominal value), 2.90 (XRF), 2.95 (EDX), and 2.30 (XPS). This result suggests a more homogeneous distribution of elements on the surface and in the bulk of  $Cs_{0.7}ZnO$ .

Similar analyses were conducted on the  $K_{0.8}ZnTO$  but it was found that the surface of this material is deficient of the Ti and Zn. This statement was deduced from the surface (Ti+Zn)/K which is as low as 1.50, <sup>34</sup> compared to the nominal value of 2.5 for  $K_{0.8}Zn_{0.4}Ti_{1.6}O_4$ .

The small concentration of surface Ti (and Zn) in the non-acidic  $K_{0.8}ZnTO$  contrasts the large concentration of surface Ti in  $Cs_{0.7}TO$ , or the homogeneous distribution of elements in  $Cs_{0.7}ZnTO$ . This result hints at the essential role of the large and polarizable  $Cs^{+}$  ions at interlayer space toward surface relaxation, in combination with the presence of the Ti vacancy sites  $\Box$  and or the substituted atom. Note that this is the surface characteristics only, since XRD/Raman spectroscopy has already confirmed the preservation of the lepidocrocite structure at the long/short range, respectively.

### 4.5) Catalytic activity

The ethanol conversion was performed over selected compositions, to further illustrate the dominating acid character in the lepidocrocite-type cesium titanate; acid sites convert ethanol to ethylene and diethyl ether, while acid-base pairs couple two molecules of ethanol into butanol (i.e., Guebert reaction). The acidic cesium titanates (as made  $Cs_{0.7}TO$ , or after ball milling  $Cs_{0.7}TO$ -BM) were chosen as a representative sample, in comparison to MgO which is well known to predominantly exhibit the basic character. Ethanol conversion and product yields as a function of time on stream in a flow reactor at 380 °C are shown in Figure 11.

The initial conversion is 7.1% (Cs<sub>0.7</sub>TO) vs 30.0% (MgO), which can be accounted for by the difference in  $S_{BET}$  (5, vs 63 m<sup>2</sup>·g<sup>-1</sup> respectively), suggesting that the observed catalytic activity is contributed mainly from the external surfaces. Moreover, the ethylene conversion was increased to 13.1% over ball-milled cesium titanate Cs<sub>0.7</sub>TO-BM where the was increased to 28 m<sup>2</sup>·g<sup>-1</sup>. In fact, the difference in ethanol conversion over Cs<sub>0.7</sub>TO-BM and MgO (30%/13% = 2.3) is the same as that in  $S_{BET}$  (63/28 = 2.3). Simply put, these samples are equally active per surface area. Future work could focus on the preparation of high-surface area cesium lepidocrocite titanates while retaining this unusually acidic surface character. (Potential synthetic methods include solid state synthesis at low temperature, <sup>80</sup> solid state combustion, <sup>81</sup> or hydrothermal synthesis.)

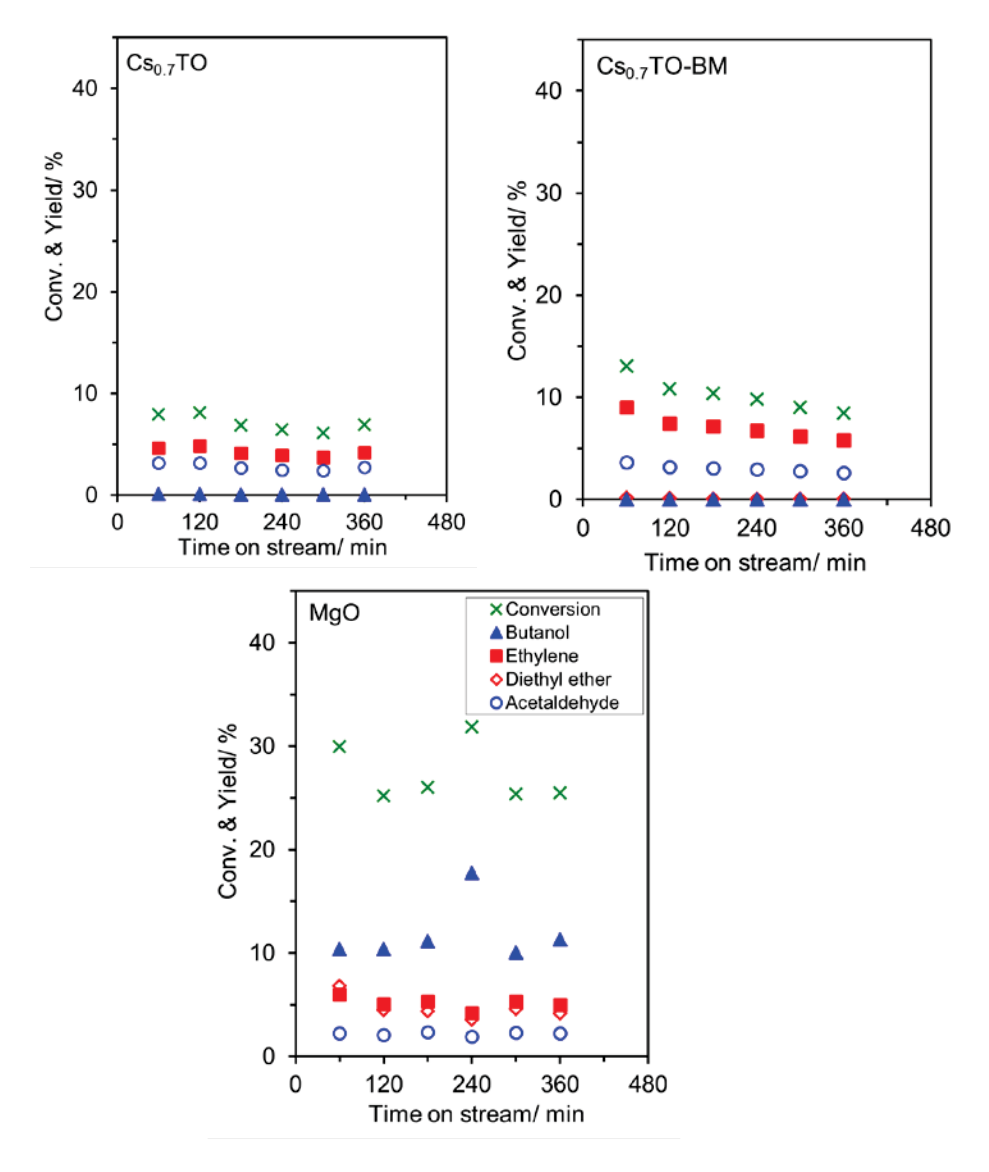


Figure 11. Conversion of ethanol and %yield of products over  $Cs_{0.7}TO$ ,  $Cs_{0.7}TO$ -BM and MgO. Reaction conditions: activation in air at 400 °C for 2 h; reaction temperature 380 °C;  $W/F = 58 \text{ g}\cdot\text{h}\cdot\text{mol}^{-1}$ ; atmospheric pressure; flow rate of carrier gas (N<sub>2</sub>) 60 mL·min<sup>-1</sup>.

Turning to product distribution, it is important to note that the major product over  $Cs_{0.7}TO$  and  $Cs_{0.7}TO$ -BM is ethylene, which could be formed over acid sites. On the other hand, butanol which is collectively formed over acid-basic pairs is the major product over MgO. (The yield of butanol is ~0.1-0.2% over  $Cs_{0.7}TO$  and  $Cs_{0.7}TO$ -BM.) Clearly, the relative abundance of acid-to-basic sites dictates the product distribution.

It is of interest to see if one can tune the acidic-basic property in this material which is characteristics of the  ${\rm Ti}^{4+}, {\rm M}^{n+}$  and the  ${\rm O}^{2-}$  sites respectively. If so, a reaction requiring the presence of two types of active sites could be selectively catalyzed. One possible approach is to tune the composition  $^{8,9,10,11,12,13,14}$  (as demonstrated here for  ${\rm Cs}_{0.7}{\rm TO}$  vs  ${\rm Cs}_{0.7}{\rm ZnO}$ ). This will benefit the transformation of more complex chemicals into value targets for e.g., functionalized monomers, pharmaceutical chemicals.

Figure 12 also compares the XRD patterns of the  $Cs_{0.7}TO$  before and after use (" $Cs_{0.7}TO$ -Spent") as a catalyst in this reaction. The layer structure is still retained despite of a halo and the slight peak broadening/a reduction in crystallite size (D=26 nm). This is presumably due to the partial desegregation of some microcrystal layers by water (*i.e.*, steaming) produced *in situ* via ethanol dehydration. Yet, the possibility to use  $Cs_{0.7}TO$  at the reaction temperature as high as 380 °C greatly expands the temperature limit from that typically employed in the protonic form (< 100 °C).  $^{26,27,28,29,30}$ 

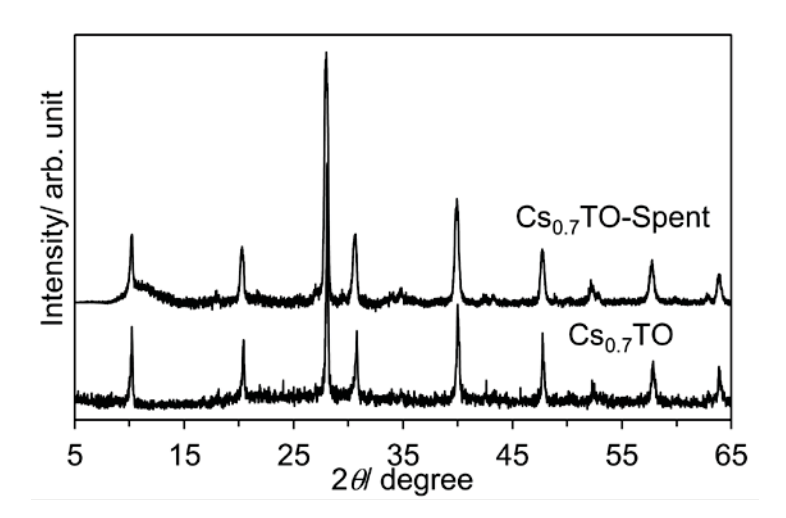


Figure 12. XRD patterns of  $Cs_{0.7}TO$  and  $Cs_{0.7}TO$ -Spent, *i.e.*, after use as a catalyst in the ethanol conversion at 380 °C for 6 h.

### 5. Conclusion and suggestions

This report showed as an example that  $Cs_xTi_{2-y}M_yO_4$  (x=0.67, 0.70;  $M=\Box$ , Zn) microcrystals were unusually acidic as compared to common metal oxides. This is exceptional for layered metal oxides since (i) protonation/ion exchange, pillaring, delamination, restacking or lengthy synthetic procedures are not required; (ii) cesium ions which are typically regarded as the promoter for basic- indeed enhance acidic-characters; and (iii) the microcrystals have low  $S_{BET}$ . The Lewis acidic nature was confirmed by IR of sorbed pyridine, and very likely relate to the distribution of  $Ti^{4+}, M^{n+}$  species on the surface as suggested by XPS. Meanwhile, the acidity depends on several factors including the presence of Ti vacancy  $\Box$ , the inductive effect of M (*i.e.,* Zn),  $S_{BET}$  and the activation temperature. The soft and polarizable cesium ions (but not the potassium analog) were found to be essential in this unusually acidic nature.

At 380 °C at  $W/F = 58 \text{ g·h·mol}^{-1}$ , the ethanol conversion was 7-13% over the cesium titanates. While this was rather low, the conversion can be improved by ball milling which reduced the particle sizes and therefore increased the  $S_{BET}$ . The production of ethylene from ethanol over  $Cs_{0.7}TO$  supports the presence of active acid sites. Therefore, the prepared materials can operate as the catalyst for ethanol-to-ethylene conversion in a manner similar to e.g.,  $TiO_2$ ,  $^{83}$   $Al_2O_3$ ,  $^{84}$  although this was at first rather unexpected considering the presence of  $Cs^+$  ions. No other cesium-containing oxides exhibit the acidic property to the best of the author's knowledge. Importantly, the lepidocrocite-type layered structure is preserved after 700 °C, contrasting the conversion to anatase at the early temperature of 450 °C in the protonic analog.

The following points were suggested for further investigations:

- 1. The influence of the composition <sup>8,9,10,11,12,13,14</sup> could be studied in depth including the variation in the metal component (and the corresponding electronegativity) at the layers and also *between* the layers.
- 2. The alkali lepidocrocite titanates reported here had quite low specific surface area. The alternative synthesis method <sup>80,81,82</sup> to yield high surface area materials will suite the catalytic applications. Once these high surface area lepidocrocite titanates are available, it will be interesting to fully optimize the reaction conditions for selectively producing ethanol, butanol, or even complexed chemicals with several functional groups. Such conditions include temperature, contact time, stability, and so on.
- 3. It is of interest whether related structures  $^{37,66,67}$  of the cesium titanate (*i.e.*, with variations in the number of repeating edge-shared octahedral such as  $Cs_2Ti_5O_{11}$ ,  $Cs_2Ti_2O_5$ ) or with completely different structure but similar component (such as the hollandite  $^{85}$   $Cs_{1.333}Zn_{0.667}Ti_{7.333}O_{16}$ ) will exhibit this unusually acidic property, including the rationale behind such behavior.

#### 6. References

- 1. van der Heijden, H.; Ptasinski, K. J. Exergy analysis of thermochemical ethanol production via biomass gasification and catalytic synthesis. *Energy* **2012**, 46, 200-210.
- 2. Balat, M.; Balat, H. Recent trends in global production and utilization of bioethanol fuel. *App. Energy* **2009**, 86, 2273-2282.
- 3. Sun, J.; Wang, Y. Recent advances in catalytic conversion of ethanol to chemicals. *ACS Catal.* **2014**, 4, 1078-1090.
- 4. Kozlowski, J. T.; Davis, R. J. Heterogeneous catalysts for the Guerbet coupling of alcohols. *ACS Catal.* **2013,** 3, 1588-1600.
- Maluangnont, T.; Arsa, P.; Limsakul, K.; Juntarachairot, S.; Sangsan, S.; Gotoh,
   K.; Sooknoi, T. Surface and interlayer base-characters in lepidocrocite titanate:
   The adsorption and intercalation of fatty acid. *J. Solid State Chem.* 2016, 238, 175-181.
- 6. Maluangnont, T.; Arsa, P.; Sooknoi, T. Extending the basic function of lattice oxygen in lepidocrocite titanate the conversion of intercalated fatty acid to liquid hydrocarbon fuels. *J. Solid State Chem.* **2017**, 256, 219-226.
- 7. Reid, A. F.; Mumme, W. G.; Wadsley, A. D. A new class of compound  $M_x^+ A_x^{3+} Ti_{2-x}O_4$  (0.60<x<0.80) typified by  $Rb_{xMn}x_Ti2-xO4$ . *Acta Cryst.* **1968**, B24, 1228-1233.
- 8. Sasaki, T.; Kooli, F.; Iida, M.; Michiue, Y.; Takenouchi, S.; Yajima, Y.; Izumi, F.; Chakoumakos, B. C.; Watanabe, M. A mixed alkali metal titanate with the lepidocrocite-like layered structure. Preparation, crystal structure, protonic form, and acid-base intercalation properties. *Chem. Mater.* **1998**, 10, 4123-4128.

- 9. Gao, T.; Fjellvåg, H.; Norby, P. Protonic titanate derived from Cs<sub>x</sub>Ti<sub>2-x/2</sub>Mg<sub>x/2</sub>O<sub>4</sub> (x
  = 0.7) with lepidocrocite-type layered structure. *J. Mater. Chem.* 2009, 19, 787-794.
- 10. Dong, X.; Osada, M.; Ueda, H.; Ebina, Y.; Kotani, Y.; Ono, K.; S, U.; Kobayashi, K.; Takada, K.; Sasaki, T. Synthesis of Mn-substituted titania nanosheets and ferromagnetic thin films with controlled doping. *Chem. Mater.* **2009**, 21, 4366-4373.
- 11. Dong, X.; Fu, J.; Xi, F. Synthesis and layer-by-layer self-assembly of titania nanosheets controllably doped with binary transition metal ions. *J. Mater. Res.* **2011**, 26, 1285-1291.
- 12. Reid, A. F.; Mumme, W. G.; Wadsley, A. D. A new class of compound  $M_x^+ A_x^{3+} Ti_{2-x}O_4$  (0.60<x<0.80) typified by  $Rb_x Mn_x Ti_{2-x}O_4$ . *Acta Cryst.* **1968**, B24, 1228-1233.
- 13. Song, H.; Sjåstad, A. O.; Vistad, Ø. B.; Gao, T.; Norby, P. Preparation of Nb-substituted titanates by a novel sol-gel assisted solid state reaction. *Inorg. Chem.* **2009**, 48, 6952-6959.
- 14. Grey, I. E.; Li, C.; Madsen, I. C.; Watts, J. A. The stability and structure of  $Cs_x[Ti_{2-x/4}\square_{x/4}]O_4$ , 0.61 < x < 0.65. *J. Solid State Chem.* **1987**, 66, 7-19.
- Busca, G. Acid catalysts in industrial hydrocarbon chemistry. *Chem. Rev.* 2007,
   5366–5410.
- 16. Zhou, C.-H.; Xia, X.; Lin, C.-X.; Tong, D.-S.; Beltramini, J. Catalytic conversion of lignocellulosic biomass to fine chemicals and fuels. *Chem. Soc. Rev.* **2011**, 40, 5588-5617.

- 17. Helwani, Z.; Othman, M. R.; Aziz, N.; Kim, J.; Fernando, W. J. N. Solid heterogeneous catalysts for transesterification of triglycerides with methanol: A review. *Appl. Catal. A* **2009**, 363, 1-10.
- 18. Su, F.; Guo, Y. Advancements in solid acid catalysts for biodiesel production. *Green Chem.* **2014**, 16, 2934-2957.
- 19. Takagaki, A.; Tagusagawa, C.; Hayashi, S.; Hara, M.; Domen, K. Nanosheets as highly active solid acid catalysts for green chemical syntheses. *Energy Env. Sci.* **2010**, 3, 82-93.
- 20. Bavykin, D. V.; Friedrich, J. M.; Walsh, F. C. Protonated titanates and TiO<sub>2</sub> nanostructured materials: Synthesis, properties, and applications. *Adv. Mater.* **2006**, 18, 2807-2824.
- 21. Tagusagawa, C.; Takagaki, A.; Hayashi, S.; Domen, K. Characterization of HNbWO<sub>6</sub> and HTaWO<sub>6</sub> Metal oxide nanosheet aggregates as solid acid catalysts. *J. Phys. Chem. C* **2009**, 113, 7831-7837.
- 22. Kooli, F.; Sasaki, T.; Watamabe, M.; Martin, C.; Rives, V. Microporosity and acidity properties of alumina pillared titanates. *Langmuir* **1999**, 15, 1090-1095.
- 23. Kooli, F.; Sasaki, T.; Mizukami, F.; Watanabe, M.; Martin, C.; Rives, V. Characterization and acidic properties of silica pillared titanates. *J. Mater. Chem.* **2001,** 11, 841-845.
- 24. Maluangnont, T.; Matsuba, K.; Geng, F.; Ma, R.; Yamauchi, T.; Sasaki, T. Osmotic swelling of layered compounds as a route to producing high-quality two-dimensional materials. A comparative study of tetramethylammonium versus

- tetrabutylammonium cation in a lepidocrocite-type titanate. *Chem. Mater.* **2013**, 25, 3137–3146.
- 25. Lee, M.; Seo, Y.; Shin, H. S.; Jo, C.; Ryoo, R. Anatase TiO<sub>2</sub> nanosheets with surface acid sites for Friedel-Crafts alkylation. *Microporous Mesoporous Mater.* **2016**, 222, 185-191.
- 26. Kitano, M.; Nakajima, K.; Kondo, J. N.; Hayashi, S.; Hara, M. Protonated titanate nanotubes as solid acid catalyst. *J. Am. Chem. Soc.* **2010,** 132, 6622-6623.
- 27. Kitano, M.; Wada, E.; Nakajima, K.; Hayashi, S.; Miyazaki, S.; Kobayashi, H.; Hara, M. Protonated titanate nanotubes with Lewis and Brønsted acidity: relationship between nanotube structure and catalytic activity. *Chem. Mater.* **2013**, 25, 385-393.
- 28. Wada, E.; Kitano, M.; Nakajima, K.; Hara, M. Effect of preparation conditions on the structural and acid catalytic properties of protonated titanate nanotubes. *J. Mater. Chem. A* **2013**, 1, 12768-12774.
- 29. Kitano, M.; Kobayashi, H.; Hayashi, S.; Hara, M. Acid properties of protonated titanate nanotubes. *J. Jpn. Petrol. Institute* **2017**, 60, 113-120.
- 30. de Carvalho, D. C.; Oliveira, A. C.; Ferreira, O. P.; Filho, J. M.; Tehuacanero-Cuapa, S.; Oliveira, A. C. Titanate nanotubes as acid catalysts for acetalization of glycerol with acetone: influence of the synthesis time and the role of structure on the catalytic performance. *Chem. Eng. J.* **2017**, 313, 1454-1467.
- 31. Sasaki, T.; Watanabe, M.; Michiue, Y.; Komatsu, Y.; Izumi, F.; Takenouchi, S. Preparation and acid-base properties of a protonated titanate with the lepidocrocite-like layer structure. *Chem. Mater.* **1995,** 7, 1001-1007.

- 32. Groult, D.; Mercey, C.; Raveau, B. Nouveaux oxydes à structure en feuillets: Les titanates de potassium non-stoechiométriques Kx(M<sub>y</sub>Ti<sub>2-y</sub>)O<sub>4</sub>. *J. Solid State Chem.* **1980,** 32, 289-296.
- 33. Gao, T.; Fjellvåg, H.; Norby, P. Defect chemistry of a zinc-doped lepidocrocite titanate  $Cs_xTi_{2-x/2}Zn_{x/2}O_4$  (x = 0.7) and its protonic form. *Chem. Mater.* **2009**, 21, 3503-3513.
- 34. Maluangnont, T.; Chanlek, N.; Suksawad, T.; Tonket, N.; Saikhamdee, P.; Sukkha, U.; Vittayakorn, N. Beyond soft chemistry bulk and surface modifications of polycrystalline lepidocrocite titanate induced by post-synthesis thermal treatment. *Dalton Trans.* **2017**, 46, 14277-14285.
- 35. Momma, K.; Izumi, F. VESTA 3 for three-dimensional visualization of crystal, volumetric and morphology data. *J. Appl. Cryst.* **2011,** 44, 1272-1276.
- 36. Yokosawa, K.; Takei, T.; Yanagida, S.; Kumada, N.; Katsumata, K. Ion exchange of layered titanate with transition metal and application to ammonia storage. *J. Ceram. Soc. Jpn.* **2018**, 126, 808-813.
- 37. Camposeco, R.; Castillo, S.; Mejia-Centeno, I.; Navarrete, J.; Rodriguez-Gonzalez, V. Behavior of Lewis and Brönsted surface acidity featured by Ag, Au, Ce, La, Fe, Mn, Pd, Pt, V and W decorated on protonated titanate nanotubes. *Microporous Mesoporous Mater.* **2016**, 236, 235-243.
- 38. Srilatha, K.; Sree, R.; Devi, B. L. A. P.; Prasad, P. S. S.; Prasad, R. B. N.; Lingaiah, N. Preparation of biodiesel from rice bran fatty acids catalyzed by heterogeneous cesium-exchanged 12-tungstophosphoric acids. *Bioresource Technol.* **2012**, 116, 53-57.

- 39. Sararuk, C.; Yang, D.; Zhang, G.; Li, C.; Zhang, S. One-step aldol condensation of ethyl acetate with formaldehyde over Ce and P modified cesium supported alumina catalyst. *Ind. Eng. Chem. Res.* **2017**, 46, 342-349.
- 40. Li, J.; Davis, R. J. On the use of 1-butene double-bond isomerization as a probe reaction on cesium-loaded zeolite X. *Appl. Catal. A* **2003**, 239, 59-70.
- 41. Davis, R. J. New perspectives on basic zeolites as catalysts and catalyst supports. *J. Catal.* **2003**, 216, 396-405.
- 42. Jiang, X.; Manawan, M.; Feng, T.; Qian, R.; Zhao, T.; Zhou, G.; Kong, F.; Wang, Q.; Dai, S.; Pan, J. H. Anatase and rutile in Evonik aroxide P25: Heterojunctioned or individual nanoparticles? *Catal. Today* **2018**, 300, 12-17.
- 43. Al-Dughaither, A. S.; de Lasa, H. HZSM-5 zeolites with different SiO<sub>2</sub>/Al<sub>2</sub>O<sub>3</sub> ratios. Characterization and NH<sub>3</sub> desorption kinetics. *Ind. Eng. Chem. Res.* **2014**, 53, 15303-15316.
- 44. Kofke, T. J. G.; Gorte, R. J.; Farneth, W. E. Stoichiometric adsorption complexes in H-ZSM-5, H-ZSM-12, and H-Mordenite zeolites. *J. Catal.* **1989**, 115, 265-272.
- 45. Parrillo, D. J.; Adamo, A. T.; Kokotailo, G. T.; Gorte, R. J. Amine adsorption in H-ZSM-5. *Appl. Catal.* **1990,** 67, 107-118.
- 46. Ko, J. E.; Kwon, B. J.; Jung, H. Synthesis and characterization of the SnO<sub>2</sub>-pillared layered titanate nanohybrid. *J. Phys. Chem. Solids* **2010**, 71, 658-662.
- 47. Choy, J.-H.; Lee, H.-C.; Jung, H.; Kim, H.; Boo, H. Exfoliation and restacking route to anatase-layered titanate nanohybrid with enhanced photocatalytic activity. *Chem. Mater.* **2002**, 14, 2486-2491.

- 48. Miura, H. CellCalc: A unit cell parameter refinement program on Windows computer. *Nippon Kessho Gakkaishi* **2003**, 45, 145-147 [in Japanese].
- 49. Sasaki, T.; Komatsu, Y.; Fujiki, Y. Protonated pentatitanate: preparation, characterizations and cation intercalation. *Chem. Mater.* **1992**, 4, 894-899.
- 50. Gao, T.; Fjellvag, H.; Norby, P. Crystal structures of titanate nanotubes: a Raman scattering study. *Inorg. Chem.* **2009**, 48, 1423-1432.
- 51. Gao, T.; Fjellvag, H.; Norby, P. Raman scattering properties of a protonic titanate  $H_xTi_{2-x/4} \square_{x/4} O_4 \cdot H_2 O$  ( $\square$ , vacancy; x=0.7) with lepidocrocite-type layered structure. *J. Phys. Chem. B* **2008**, 112, 9400-9405.
- 52. Adar, F. Molecular Spectroscopy Workbench Raman Spectra of Metal Oxides.

  Spectroscopy 2014, 29, 14-+.
- 53. Kouva, S.; Kanervo, J.; Schü $\beta$ ler, F.; Olindo, R.; Lercher, J. A.; Krause, O. Sorption and diffusion parameters from vacuum-TPD of ammonia on H-ZSM-5. *Chem. Eng. Sci.* **2013**, 89, 40-48.
- 54. Gorte, R. J. Temperature-programmed desorption for the characterization of oxide catalysts. *Catal. Today* **1996**, 28, 405-414.
- 55. Gorte, R. J. Design parameters for temperature programmed desorption from porous catalysts. *J. Catal.* **1982**, 75, 164-174.
- 56. Sanderson, R. T. Electronegativity and bond energy. *J. Am. Chem. Soc.* **1983**, 105, 2259-2261.
- 57. Sanderson, R. T. Electronegativity and bonding of transitional elements. *Inorg. Chem.* **1986**, 25, 3518-3522.

- 58. Wang, H.; Song, Y.; Xiong, J.; Bi, J.; Li, L.; Yu, Y.; Liang, S.; Wu, L. Highly selective oxidation of furfuryl alcohol over monolayer titanate nanosheet under visible light irradiation. *Appl. Catal. B* **2018**, 224, 394-403.
- 59. Ohwada, M.; Kimoto, K.; Mizoguchi, T.; Ebina, Y.; Sasaki, T. Atomic structure of titania nanosheet with vacancies. *Sci. Rep.* **2013**, 3, 2801.
- 60. Ohwada, M.; Kimoto, K.; Suenaga, K.; Sato, Y.; Ebina, Y.; Sasaki, T. Synthesis and atomic characterization of a Ti<sub>2</sub>O<sub>3</sub> nanosheet. *J. Phys. Chem. Lett.* **2011,** 2, 1820-1823.
- 61. Zhao, L.; An, H.; Zhao, X.; Wang, Y. TiO<sub>2</sub>-catalyzed *n*-valeraldehyde self-condensation to 2-propyl-2-heptenal: acid catalysis or base catalysis? *Ind. Eng. Chem. Res.* **2016,** 55, 12326-12333.
- 62. Manriquez, M. E.; López, T.; Gómez, R.; Navarrete, J. Preparation of TiO<sub>2</sub>-ZrO<sub>2</sub> mixed oxides with controlled acid-basic properties. *J. Mol. Catal. A* **2004,** 220, 229-237.
- 63. Quesada, J.; Arreola-Sánchez, R.; Faba, L.; Díaz, E.; Rentería-Tapia, V. M.; Ordóñez, S. Effect of Au nanoparticles on the activity of TiO<sub>2</sub> for ethanol upgrading reactions. *Appl. Catal. A* **2018**, 551, 23-33.
- 64. Smirniotis, P. G.; Sreekanth, P. M.; Peña, D. A.; Jenkins, R. G. Manganese oxide catalysts supported on TiO<sub>2</sub>, Al<sub>2</sub>O<sub>3</sub>, and SiO<sub>2</sub>: a comparison for low-temperature SCR of NO with NH<sub>3</sub>. *Ind. Eng. Chem. Res.* **2006**, 45, 6436-6443.
- 65. Li, S.; Li, N.; Li, G.; Li, L.; Wang, A.; Cong, Y.; Wang, X.; Xu, G.; Zhang, T. Protonated titanate nanotubes as a highly active catalyst for the synthesis of renewable diesel and jet fuel range alkanes. *Appl. Catal. B* **2015**, 170-171, 124-134.

- 66. Madarász, D.; Szenti, I.; Nagy, L.; Sápi, A.; Kukovecz, A.; Kónya, Z. Fine tuning the surface acidity of titanate nanostructures. *Adsorption* **2013**, 19, 695-700.
- 67. Reddy, B. R. P.; Reddy, P. V. G.; Kumar, D. P.; Reddy, B. N.; Shankar, M. V. Rapid synthesis of alkylaminophenols *via* the Petasis borono-Mannich reaction using protonated trititanate nanotubes as robust solid-acid catalysts. *RSC Adv.* **2016**, 6, 14682-14691.
- 68. Camposeco, R.; Castillo, S.; Mejía-Centeno, I.; Navarrete, J.; Nava, N. Boosted surface acidity in TiO<sub>2</sub> and Al<sub>2</sub>O<sub>3</sub>-TiO<sub>2</sub> nanotubes as catalytic supports. *Appl. Surf. Sci.* **2015,** 356, 115-123.
- 69. Bao, N.; Shen, L.; Yanagisawa, K. Textural and catalytic properties of combinatorial micro-mesoporous octatitanate fibers prepared by solvothermal soft chemical process. *J. Phys. Chem. B* **2004**, 108, 16739-16745.
- 70. Uchida, Y.; Hara, M.; Funatsu, A.; Shimojo, F. Electronic structure of titania nanosheets with vacancies based on first-principles calculations. *e-J. Surf. Sci. Nanotech.* **2018**, 16, 1-4.
- 71. Grey, I. E.; Wilson, N. C. Titanium vacancy defects in sol-gel prepared anatase. *J. Solid State Chem.* **2007**, 180, 670-678.
- 72. Foo, G. S.; Polo-Garzon, F.; Fung, V.; Jiang, D.-E.; Overbury, S. H.; Wu, Z. Acid-base reactivity of perovskite catalysts probed via conversion of 2-propanol over titanates and zirconates. *ACS Catal.* **2017**, 7, 4423-4434.
- 73. Kapustin, G. I.; Brueva, T. R.; Klyachko, A. L.; Beran, S.; Wichterlova, B. Determination of the number and acid strength of acid sites in zeolites by ammonia

- adsorption. Comparison of calorimetry and temperature-programmed desorption of ammonia. *Appl. Catal.* **1988**, 42, 239-246.
- 74. Shetsiri, S.; Thivasasith, A.; Saenluang, K.; Wannapakdee, W.; Salakhum, S.; Wetchasat, P.; Nokbin, S.; Limtrakul, J.; Wattanakit, C. Sustainable production of ethylene from bioethanol over hierarchical ZSM-5 nanosheets. *Sustainable Energy Fuels* **2019,** 3, 115-126.
- 75. Bezrodna, T.; Puchkovska, G.; Shimanovska, V.; Chashechnikova, I.; Khalyavka, T.; Baran, J. Pyridine-TiO<sub>2</sub> surface interaction as a probe for surface active centers analysis. *Appl. Surf. Sci.* **2003**, 214, 222-231.
- 76. Gao, T.; Norby, P.; Okamoto, H.; Fjellvåg, H. Syntheses, structures, and magnetic properties of nickel-doped lepidocrocite titanates. *Inorg. Chem.* **2009**, 48, 9409-9418.
- 77. Pilarski, M.; Marschall, R.; Gross, S.; Wark, M. Layered cesium copper titanate for photocatalytic hydrogen production. *Appl. Catal. B* **2018**, 227, 349-355.
- 78. Zhang, M.; Yu, Y. Dehydration of ethanol to ethylene. *Ind. Eng. Chem. Res.* **2013,** 52, 9505-9514.
- 79. Idriss, H.; Seebauer, E. G. Reactions of ethanol over metal oxides. *J. Mol. Catal.*A 2000, 152, 201-212.
- 80. Ogawa, M.; Morita, M.; Igarashi, S.; Sato, S. A green synthesis of a layered titanate, potassium lithium titanate; Lower tempeature solid-state reaction and improved materials performance. *J. Solid State Chem.* **2013**, 206, 9-13.

- 81. Yin, S.; Zhang, W.; Xue, L.; Yan, Y. Effects of reaction parameters on solution combustion synthesis of lepidocrocite-like K<sub>0.80</sub>Ti<sub>1.733</sub>Li<sub>0.267</sub>O<sub>4</sub>: Phase formation and morphology evaluation. *J. Mater. Sci.* **2013**, 48, 1533-1542.
- 82. Masaki, N.; Uchida, S.; Sato, T. Moderate hydrothermal synthesis of layered caesium titanium. *J. Mater. Chem.* **2002**, 12, 305-308.
- 83. Carrizosa, I.; Munuera, G. Study of the interaction of aliphatic alcohols with TiO<sub>2</sub> I. Decomposition of ethanol, 2-propanol, and tert-butanol on anatase. *J. Catal.* **1977,** 49, 174-188.
- 84. Lee, J.; Szanyi, J.; Kwak, J. H. Ethanol dehydration on **γ**-Al<sub>2</sub>O<sub>3</sub>: effects of partial pressure and temperature. *Mol. Catal.* **2017**, 434, 39-48.
- 85. Grote, R.; Zhao, M.; Shuller-Nickles, L.; Amoroso, J.; Gong, W.; Lilova, K.; Navrotsky, A.; Tang, M.; Brinkman, K. S. Compositional control of tunnel features in hollandite-based ceramics: structure and stability of (Ba,Cs)<sub>1.33</sub>(Zn,Ti)<sub>8</sub>O<sub>16</sub>. *J. Mater. Sci.* **2019,** 54, 1112-1125.

### 7. Output

This research funded by Thailand Research Fund, grant number MRG6080004, has resulted in the following outputs.

### 7.1) International journal publications

Maluangnont, T.; Wuttitham, B.; Hongklai, P.; Khunmee, P.; Tippayasukho, S.; Chanlek, N.; Sooknoi, T. "An unusually acidic and thermally stable cesium titanate  $Cs_xTi_{2-y}M_yO_4$  (x = 0.67 or 0.70; M = vacancy or Zn)" *Inorg. Chem.* **2019**, 58, 6885-6892.

[2018 Impact Factor = 4.85; Q1 in Inorganic Chemistry; Q1 in Chemistry (miscellaneous)]

### 7.2) Oral/poster presentations

January 9-11, 2019

"Unusually acidic and thermally stable lepidocrocite-type layered alkali titanate microcrystals for the production of ethylene from bioethanol", The 18<sup>th</sup> TRF-OHEC Annual Congress (TOAC2019), The Regent Cha-am Beach Resort, Petchburi, Thailand.

December 10-14, 2018

"Lepidocrocite-type layered titanate as a catalyst for the conversion of biomass-derived chemicals into value-added products", The International Symposium on Catalysis and Fine Chemicals 2018 (C&FC2018), Bangkok, Thailand.

### 7.3) Personnel training

This project was carried out partly by Panisa Hongklai, Pongsatorn Khunmee, and Sorawat Tippayasukho. They were the undergraduates at the Department of Chemistry, Faculty of Science, KMITL at that time. Ms. Panisa Hongklai is currently a Master's student at KMITL. In addition, this project was assisted in part by Boonyawat Wuttitham who was and remains the Ph.D. student at the same affiliation.

A1. ผลงานตีพิมพ์ที่ได้จากโครงการ

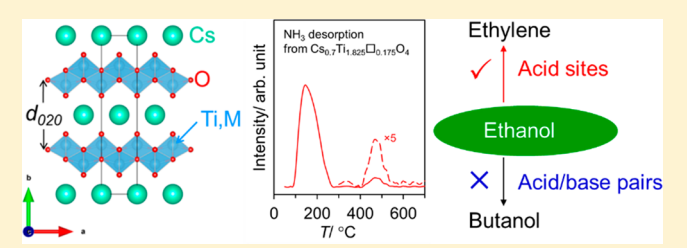
pubs.acs.org/IC

# An Unusually Acidic and Thermally Stable Cesium Titanate $Cs_xTi_{2-v}M_vO_4$ (x = 0.67 or 0.70; M = vacancy or Zn)

Tosapol Maluangnont,\*,†,‡® Boonyawat Wuttitham,§ Panisa Hongklai,§ Pongsatorn Khunmee,§ Sorawat Tippayasukho,<sup>§</sup> Narong Chanlek,<sup>||</sup> and Tawan Sooknoi\*, <sup>‡, §</sup>

Supporting Information

ABSTRACT: Proton-free, alkali-containing layered metal oxides are thermally stable compared to their protonic counterparts, potentially allowing catalysis by Lewis acid sites at elevated temperatures. However, the Lewis acidic nature of these materials has not been well explored, as alkali ions are generally considered to promote basic but to suppress acidic character. Here, we report a rare example of an unusually acidic cesium-containing oxide  $Cs_xTi_{2-\nu}M_{\nu}O_4$  (x = 0.67 or 0.70; M = Ti vacancy ☐ or Zn). These lepidocrocite-



type microcrystals desorbed NH<sub>3</sub> at >400 °C with a total acidity of  $\lesssim$ 410  $\mu$ mol g<sup>-1</sup> at a specific surface area of only 5 m<sup>2</sup> g<sup>-1</sup>, without the need for lengthy proton-ion exchange, pillaring, delamination, or restacking. The soft and easily polarized Cs+ ion essentially drives the formation of the Lewis acidic site on the surfaces as suggested by IR of sorbed pyridine. The twodimensional layered structure was preserved after the oxide was employed in the ethanol conversion at 380 °C, the temperature at which the protonic form could have converted to anatase. The structure was also retained after the NH3 temperatureprogrammed desorption measurement up to 700 °C. The production of ethylene from ethanol, well-known to occur over acid sites, unambiguously confirmed the acidic nature of this cesium titanate.

### ■ INTRODUCTION

Acidic materials of the Brønsted (proton-donating) or Lewis type (electron-accepting) are of paramount importance in industrial hydrocarbon chemistry, biomass conversion, and synthesis of fine chemicals.<sup>2-4</sup> Recently, protonated layered metal oxides (e.g., titanates and niobates) have received an increasing amount of attention due to their compositional, structural, and microstructural tunability. 5-7 The Brønsted acidic properties depend on their two-dimensional (2D) nature, where protons from the medium exchange with the interlayer cations and are incorporated in the gallery. On the other hand, the Lewis acidic properties that originated from the electron-deficient species, either at the interlayer or at the sheets, have been explored much less.

To prepare 2D materials with Brønsted acid sites accessible to probe molecules or reactants, proton exchange of such solids is typically followed by pillaring, 8,9 delamination, 10 and restacking<sup>5</sup> or the synthesis is conducted in the presence of a structure-directing agent.<sup>11</sup> Otherwise, they typically exhibit low acidity as a result of relatively large particles often in the form of microcrystals. In addition, the low thermal stability of the layered structure containing Brønsted sites limits the

application window to relatively mild reaction temperatures, mostly <100 °C. 12-16 For example, Sasaki et al. 17 reported that the lepidocrocite-type  $H_x Ti_{2-x/4} \square_{x/4} O_4 \cdot H_2 O$  (x = 0.7, and  $\square$ = Ti vacancy;  $H_{0.7}TO$ ) layered crystals transformed to anatase at 450 °C with an extensive mass loss of ~15 wt %. If the protonic form was pillared with aluminum polyoxocations, the layered structure was stable up to 500 °C, at which point Brønsted acid sites disappeared while Lewis acid sites remained. A similar decomposition and layered collapse was also observed  $^{16}$  in the structurally related  $H_2Ti_3O_7$  nanotubes.

These shortcomings in protonic layered titanates prompt us to investigate the possibility of developing a proton-free, Lewis acidic material. It is well-known that lepidocrocite-type alkali titanate118-21 is structurally robust and that the 2D layered structure is preserved even upon being heated ~100 °C above the synthetic temperature. 22 Lepidocrocite titanate has a general composition of  $A_x Ti_{2-y} M_y O_4$  (i.e.,  $xA^+$ )  $[Ti_{2-y}M_yO_4]^{x-}$ ), where x = y(4 - n) is the nominal charge per formula unit; n < 4 is the oxidation state of M, and n = 0

Received: February 8, 2019 Published: May 1, 2019



<sup>&</sup>lt;sup>†</sup>College of Nanotechnology, King Mongkut's Institute of Technology Ladkrabang, Bangkok 10520, Thailand

<sup>&</sup>lt;sup>‡</sup>Catalytic Chemistry Research Unit, Faculty of Science, King Mongkut's Institute of Technology Ladkrabang, Bangkok 10520, Thailand

<sup>§</sup>Department of Chemistry, Faculty of Science, King Mongkut's Institute of Technology Ladkrabang, Bangkok 10520, Thailand  $^{\parallel}$ Synchrotron Light Research Institute (Public Organization), 111 University Avenue, Muang District, Nakhon Ratchasima 30000, Thailand

for  $M = \square$ . In this structure, the corrugated double-edge-shared  $(Ti,M)O_6$  octahedra join with negatively charged sheets, extend through the a-c (basal) plane, and stack along the b-direction. The sheets are staggered such that  $b = 2d_{020}$ , with  $A^+$  ions situated in the interlayer space (see Figure 1a,b). The Ti/M atoms potentially serve as the Lewis acid sites, especially if they are on the accessible surfaces.

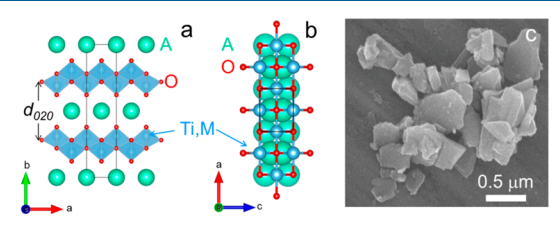


**Figure 1.** Crystal structure of  $A_xTi_{2-y}M_yO_4$  shown (a) as a polyhedral representation on the a-b plane and (b) as a ball-and-stick model on the a-c plane. Crystal structures were drawn with VESTA.<sup>23</sup> (c) Representative scanning electron microscopy image of  $Cs_{0.7}TO$ .

Our design principle is that the acidic nature of a proton-free lepidocrocite titanate could be tuned by the inductive effect of both M at the sheets and the interlayer A cations. If so, a Lewis acidic material (i.e., relative to the pristine, unmodified composition) capable of withstanding high temperatures (relative to the protonic form) might be obtained. Reports of such modifications, however, are rather limited. Relevant examples include the ion exchange of  $H_{0.7}TO$  with an aqueous solution of the metal ions<sup>24</sup> or the deposition of metal nanoparticles onto the surfaces of  $H_2Ti_3O_7$  nanotubes, <sup>25</sup> yet the enhanced acidic nature has not been fully demonstrated.

Quite unexpectedly, we found in this work that the cesium titanates  $Cs_xTi_{2-x/4}\square_{x/4}O_4$  (x = 0.67 or 0.70;  $M = \square$ ;  $Cs_xTO$ ) and  $Cs_xTi_{2-x/2}Zn_{x/2}O_4$  (x = 0.70;  $Cs_{0.7}ZnTO$ ), directly obtained right after solid state synthesis, were unusually acidic without the need for proton-ion exchange, pillaring, delamination, or restacking. These results provide an interesting example contrasting the general view that soft/ polarizable cesium ions suppress acidic while promoting basic character. 26-29 Acidity and the acidic nature of the microcrystals of these compositions were evaluated by NH3 and isopropylamine temperature-programmed desorption (TPD), Fourier transform infrared spectroscopy of adsorbed pyridine, and X-ray photoelectron spectroscopy (XPS). Effects of the Ti vacancy sites and activation temperature on acidity, including the stability of the cesium titanate, were also investigated. Consistent with the observed acid function, the catalytic activity of the cesium titanate  $Cs_xTi_{2-x/4}\square_{x/4}O_4$  toward conversion of ethanol is highlighted.

#### **■ EXPERIMENTAL SECTION**

**Synthesis.** The samples were prepared following the reported procedure,  $^{17,19,21}$  by first calcining the stoichiometric mixture of  $A_2CO_3$  (A = K or Cs), anatase-type  $TiO_2$ , and ZnO (when necessary) at  $800\,^{\circ}C$  for 1 h for decarbonation. Next, the mixture was ground and subjected to two cycles of calcination (20 h each) at  $800\,^{\circ}C$  ( $Cs_{0.7}Ti_{1.825} \square_{0.175}O_4$ ,  $Cs_{0.7}TO$ ),  $^{17}$  900 °C ( $K_{0.8}Zn_{0.4}Ti_{1.6}O_4$ ,  $K_{0.8}ZnTO$ ),  $^{19}$  or 950 °C ( $Cs_{0.7}Zn_{0.35}Ti_{1.65}O_4$ ,  $Cs_{0.7}ZnTO$ ),  $^{21}$  all with intermediate grinding. For  $Cs_{0.67}Ti_{1.8325} \square_{0.1675}O_4$  ( $Cs_{0.67}TO$ ), nanosized P25  $TiO_2^{\phantom{0}30}$  (Degussa, 99.70%) was used as the Ti source instead of anatase to increase the specific surface area. Proton exchange of  $Cs_{0.7}TO$  to  $H_{0.7}Ti_{1.825} \square_{0.175}O_4 \cdot H_2O$  ( $H_{0.7}TO$ ) was done three times at room temperature (RT) with 1 M HCl, following the

reported method<sup>17</sup> with the acid renewed each day. The resulting material was dried overnight at room temperature. All materials synthesized in this work were characterized as described in detail in the Supporting Information.

**Temperature-Programmed Desorption.** For NH $_3$  TPD, ~0.2 g of the sample was loaded into the center of a quartz tube reactor and covered with quartz wool. The sample was activated at  $T_a$  values of 300, 400, and 500 °C for 2 h and cooled to ~30 °C (both under air flowing at a rate of 10 °C min $^{-1}$ ), followed by the adsorption of 1% NH $_3$ /He (50 mL min $^{-1}$ ) for 1 h. Then, physisorbed NH $_3$  was purged with helium (30 mL min $^{-1}$ ) until the baseline as detected by the thermal conductivity detector was flat, usually for 1 h. The profile was next collected from 50 to 700 °C (10 °C min $^{-1}$ ) under a flow of helium. The acidity is expressed as micromoles of NH $_3$  per gram of the solid, which was quantified by comparison to H-ZSM-5 (PZ-2/1000H, Zeochem; nominal Si/Al = 500). See the Supporting Information for details.

Isopropylamine (IPA) TPD, which is specific to only Brønsted acid sites,  $^{31,32}$  was performed as follows. An aliquot of 1  $\mu L$  of IPA was repeatedly injected, at RT, onto 0.1 g of  $Cs_{0.7}TO$  (activated at 400 °C under air) under the flow of He (30 mL min $^{-1}$ ). The total amount of injected IPA was 10  $\mu L$ . Then, the purging and temperature-programmed desorption was conducted as described above for NH $_3$ TPD. Propylene, which is the decomposition product of IPA over Brønsted acid sites, was detected by a flame ionization detector (FID). A similar experiment was performed with H-ZSM-5.

Catalytic Activity Testing. The sample (pressed and sieved to the 600–850  $\mu$ m fraction) was packed into a vertical glass tube reactor and covered with glass wool and glass beads. Prior to activity testing, the sample was heated from RT to 400 °C (10 °C min<sup>-1</sup>), held for 2 h, and cooled to 380 °C (all under air flowing at a rate of 30 mL min<sup>-1</sup>). Then, 99.99% absolute ethanol (Carlo Erba) was fed into the reactor by a syringe pump at a rate of 1 mL h<sup>-1</sup>. N<sub>2</sub> was used as a carrier gas at a rate of 60 mL min<sup>-1</sup>, corresponding to a contact time (W/F) of 58 g h mol<sup>-1</sup>. The catalytic testing was conducted for a total time on stream of 6 h. The products were periodically analyzed using an online BUCK Scientific 910 gas chromatograph equipped with the FID and the FFAP column (30 m × 0.25 mm × 0.25  $\mu$ m), by comparison with the retention time and peak area of the standard at a known concentration.

#### ■ RESULTS AND DISCUSSION

**Structural Characteristics.** The samples are white, platelike microcrystals with a particle size of  $\sim$ 0.5  $\mu$ m as shown in Figure 1c for Cs<sub>0.7</sub>TO as a representative. Figure 2 shows the X-ray diffraction (XRD) patterns of the investigated

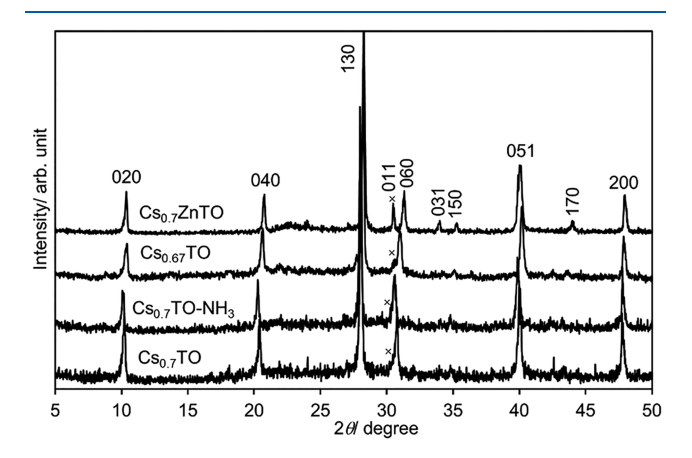


**Figure 2.** XRD patterns of the cesium titanate samples investigated in this work, including the respective hkl indices shown atop the peak. The times signs denote the 011 reflections that overlap or separate from the nearby 060 reflection, depending on the composition. <sup>18,21</sup>

Table 1. Unit Cell Parameters of the Samples

	a (Å)	b (Å)	c (Å)	ref
$Cs_{0.7}TO (Cs_{0.7}Ti_{1.825}\square_{0.175}O_4)$	3.815(4)	17.46(2)	2.961(6)	this work
	3.837(1)	17.198(3)	2.960(1)	17
Cs <sub>0.7</sub> TO-NH <sub>3</sub> (after NH <sub>3</sub> TPD)	3.819(5)	17.54(5)	2.957(3)	this work
$Cs_{0.67}TO (Cs_{0.67}Ti_{1.8325}\square_{0.1675}O_4)$	3.803(4)	17.38(2)	2.939(7)	this work
	3.823	17.215	2.955	33, 34
$Cs_{0.7}Zn_{0.35}TO (Cs_{0.7}Zn_{0.35}Ti_{1.65}O_4)$	3.7949(8)	17.12(6)	2.974(1)	this work
	3.8143(1)	17.0205(4)	2.9837(1)	21
$K_{0.8}ZnTO (K_{0.8}Zn_{0.4}Ti_{1.6}O_4)$	3.809(3)	15.67(1)	2.981(2)	36, 38
$H_{0.7}TO (H_{0.70}Ti_{1.825} \square_{0.175}O_4 \cdot H_2O)$	3.790(3)	18.43(3)	2.953(5)	this work
	3.783(2)	18.735(8)	2.978(2)	17

samples that are all characteristics of the lepidocrocite-type cesium titanate (Immm). The 011 reflection (x in Figure 2) typically overlaps with the 060 reflection in the □-containing sample  $Cs_xTO$  (x = 0.70 or 0.67), which is in agreement with the report<sup>18</sup> by Grey et al. Upon substitution of Zn for Ti in Cs<sub>0.7</sub>ZnTO, these two peaks are clearly separated; this finding is also consistent with the calculated XRD pattern reported by Gao et al.<sup>21</sup> Table 1 lists the corresponding unit cell parameters, which agree reasonably with the reported values. 17,21,33,34 (The differences might be due to small variations in stoichiometries from different laboratories.) Taking Cs<sub>0.7</sub>TO as an example, we used CellCalc<sup>35</sup> to determine the following unit cell parameters: a = 3.815(4)Å, b = 17.46(2) Å, and c = 2.961(6) Å, with an interlayer spacing  $d_{020}$  (=b/2) of ~8.6 Å. This distance in Cs<sub>0.7</sub>TO is >7.8 Å in the potassium analogue  $K_{0.8}$ ZnTO<sup>19,22,36</sup> but is <9.4 Å in the related structure, e.g., Cs<sub>2</sub>Ti<sub>5</sub>O<sub>11</sub>.<sup>3</sup>

**Thermal Stability.** Figure 2 also compares the XRD patterns of  $Cs_{0.7}TO$  to those of  $Cs_{0.7}TO$ -NH<sub>3</sub> (i.e., after the NH<sub>3</sub> TPD measurement where a temperature of ≤700 °C was reached). Importantly, the similarity in these two patterns suggests the preservation of the lepidocrocite-type structure. Using the full width at half-maximum of the 020 peak and the Scherrer equation, an almost identical crystallite size D was obtained (42 nm for  $Cs_{0.7}TO$  and 38 nm for  $Cs_{0.7}TO$ -NH<sub>3</sub>), also indicating minimal structural changes. In addition, the Raman spectra of the two samples shown in Figure 3a are generally similar and show bands characteristic  $^{39,40}$  of the lepidocrocite-type cesium titanate. These bands are typically assigned to the Ti–O stretching vibration of the layers.  $^{39,40}$  The preservation of the peak at 914–917 cm<sup>-1</sup> due to Cs–O stretching  $^{39,40}$  in particular suggests that  $Cs^+$  ions persist in a

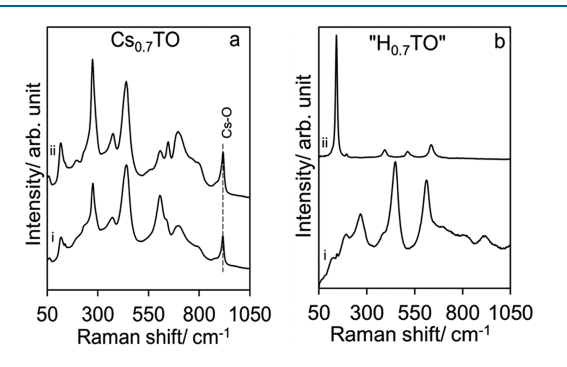
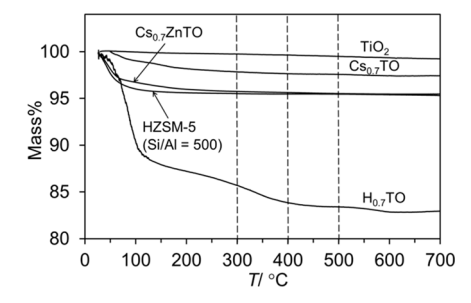


Figure 3. Raman spectra of (a)  $Cs_{0.7}TO$  and (b)  $H_{0.7}TO$ , either (i) prior to or (ii) after the NH<sub>3</sub> TPD measurement where a temperature of  $\leq$ 700 °C was reached.

similar local environment, either prior to or after the NH<sub>3</sub> TPD measurement

For comparison, the protonic form  $H_{0.7}TO$  (i.e.,  $H_{0.70}Ti_{1.825}\Box_{0.175}O_4\cdot H_2O$ ) was prepared via repeated equilibration of  $Cs_{0.7}TO$  with HCl. The XRD pattern of  $H_{0.7}TO$  and the corresponding unit cell parameters shown in Figure S1a and Table 1, respectively, agree with the literature. This material with the expanded interlayer separation ( $d_{020} = b/2 \sim 9.2 \text{ Å}$ ) contains the interlayer Brønsted acid sites and the water molecule. Characteristic Raman vibrations TPD measurement, the characteristic Raman vibrations of the protonic lepidocrocite ( $H_{0.7}TO$ ) completely disappeared as shown in Figure 3b. Instead, several peaks indicative of anatase-type  $TiO_2^{43}$  are visible, confirming the lepidocrocite-to-anatase transformation.

Such a limited thermal stability of  $H_{0.7}TO$  can also be deduced from the massive mass loss [~15 wt % (Figure 4)]



**Figure 4.** Mass loss curve of several samples recorded under  $N_2$ . The dashed lines at 300, 400, and 500 °C indicate the activation temperature  $T_{\rm a}$  where the NH $_3$  TPD measurements were carried out.

upon heating to 700 °C in a separate thermogravimetric analysis. This mass loss has been ascribed  $^{17}$  to dehydration and dehydroxylation, accompanied by the subsequent collapse of the lepidocrocite-type layers and the condensation to anatase. On the other hand, several compositions of the cesium titanate show a limited loss ( $\sim$ 2.5–5.0 wt %), which is ascribed to the liberation of water on the external surfaces. Altogether, these results highlight the superior thermal stability of the cesium analogue with respect to the protonic form.

**Acid Strength and Acidity.** The acid strength and acidity of the titanate were first investigated by NH $_3$  TPD after activation of the samples at 400 °C, where the contribution from surface water can be excluded (Figure 4). The variation in maximum peak temperature  $T_{\rm m}$  was within 10 °C, while the accuracy in acidity was ~15% (see the Supporting Information for details).

As shown in Figure 5, the  $Cs_{0.7}TO$  with Ti vacancy  $\square$  desorbs  $NH_3$  in two ranges at 100-300 °C (low-temperature,

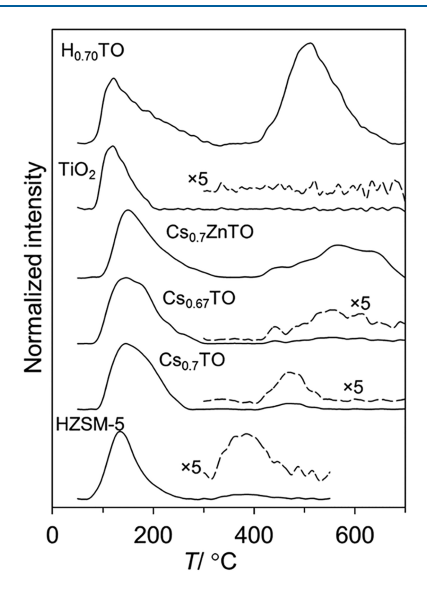


**Figure 5.** NH<sub>3</sub> TPD profiles from the samples activated at 400 °C. The profiles were normalized so that the LT peak is of the same height. Dashed lines in the HT range are magnified by a factor of 5.

LT) and >400 °C (high-temperature, HT). The respective  $T_{\rm m}$  values are ~145 and 470 °C. Similar behavior was observed in other compositions tested but with a higher  $T_{\rm m}$ , including Cs<sub>0.67</sub>TO (also with  $\square$ ) and Cs<sub>0.7</sub>ZnTO [where the  $\square$  sites were filled with Zn (see below)]. While it is well-known that  $T_{\rm m}$  is sensitive to several parameters, the desorption of NH<sub>3</sub> from the cesium titanate samples at >400 °C strongly suggests the presence of strong acid sites. The increased acidic strength of Cs<sub>0.7</sub>ZnTO (i.e., a higher  $T_{\rm m}$  especially in the HT range) might be explained by the electron-withdrawing effect of Zn, as inferred from Sanderson's electronegativity 47,48 (2.223 for Zn and 1.50 for Ti). Considering that the intercalated NH<sub>3</sub> in Co<sup>2+</sup>-exchanged H<sub>0.7</sub>TO was earlier released at <300 °C, 24 our results demonstrate the remarkable acidic nature of the cesium titanate.

The acidic strength of these cesium titanates appears to be higher than that observed in relevant samples. It was found that anatase-type  ${\rm TiO_2}$  desorbs  ${\rm NH_3}$  only at the LT ( $T_{\rm m} \sim 130$  °C) without any HT peak. Even for HZSM-5 ( ${\rm Si/Al}=500$ ), its LT desorption and HT desorption occur at a temperature slightly lower than that from the cesium titanate samples. For the protonic  ${\rm H_{0.7}TO}$  with Brønsted acid sites, the layer collapse and structural transformation  $^{17}$  (as deduced from the mass loss curve in Figure 4) certainly contribute to the desorption profile, including that reported previously. Therefore, the acidic nature of  ${\rm H_{0.7}TO}$  will not be discussed further.

Table 2 summarizes the total acidity, which is a combination of LT and HT acidity. At an activation temperature of 400  $^{\circ}$ C, the acidity of Cs<sub>0.7</sub>TO (~280  $\mu$ mol g<sup>-1</sup>) is ~5 times larger than that of TiO<sub>2</sub> with a similar S<sub>BET</sub>. The small specific surface area S<sub>BET</sub> (here ~5–6 m² g<sup>-1</sup>) is rather common for the samples prepared via a traditional, high-temperature solid state synthesis with the micrometer-sized TiO<sub>2</sub> as the reactant. It indicates that the microcrystals are essentially regarded as nonporous materials and that N<sub>2</sub> adsorption/desorption would mostly occur at the external surfaces. Therefore, the high acidity observed for Cs<sub>0.7</sub>TO despite a low S<sub>BET</sub> suggests NH<sub>3</sub> adsorption at the internal surfaces (i.e., intercalation), requiring *in situ* XRD for further characterization.

The acidity of the  $\square$ -containing  $Cs_{0.7}TO$  is also found to increase with a decrease in activation temperature  $T_a$ , reaching ~410  $\mu$ mol g<sup>-1</sup> at  $T_a$  = 300 °C as summarized in Table 2 (entries 1a–1c). This behavior is in sharp contrast to  $TiO_2$  exhibiting a relatively constant (but low) acidity at  $T_a$  values of 400 and 700 °C (entries 5a and 5b). [The acidity of  $TiO_2$  reported here is within the range of literature values (Table S1).] A different HT desorption pattern for  $Cs_{0.7}TO$  activated at different temperature (Figure 6a) suggests a complex alteration of surface functionals (e.g., Ti vacancy  $\square$ ) or surface rearrangement.  $^{22,50,51}$  In situ surface analyses will be required to test these hypotheses. The acidity increased in part with an increase in  $S_{BET}$ , as demonstrated for  $Cs_{0.67}TO$  prepared from the nanosized  $^{30}$  P25  $TiO_2$  (Table 2, entry 2).

When the Ti vacancy sites ( $\square$ ) were filled by Zn,<sup>21</sup> the total acidity of Cs<sub>0.7</sub>ZnTO is decreased to half of that of Cs<sub>0.7</sub>TO at a similar S<sub>BET</sub> (Table 2). For example at an activation temperature of 300 °C, the LT acidity and HT acidity are 100 and 108  $\mu$ mol g<sup>-1</sup>, respectively, for Cs<sub>0.7</sub>ZnTO but 347 and 64  $\mu$ mol g<sup>-1</sup>, respectively, for Cs<sub>0.7</sub>TO. This behavior was observed at all  $T_a$  values studied as also shown in Figure 6b

Table 2. Summary of Specific Surface Areas ( $S_{\rm BET}$ ), Acidities at Low (LT) and High Temperatures (HT), Including the Maximum Peak Temperature  $T_{\rm m}$ , and Total Acidities As Determined by NH<sub>3</sub> TPD

entry	sample <sup>a</sup>	$S_{\rm BET}~(\rm m^2~g^{-1})$	LT acidity ( $\mu$ mol g <sup>-1</sup> ) [ $T_{\rm m}$ (°C)]	HT acidity ( $\mu$ mol g <sup>-1</sup> ) [ $T_{\rm m}$ (°C)]	total acidity ( $\mu$ mol g <sup>-1</sup> )	
1a	Cs <sub>0.7</sub> TO-300	5	347 [143]	64 [418]	410	
1b	Cs <sub>0.7</sub> TO-400	5	264 [145]	15 [470]	279	
1c	Cs <sub>0.7</sub> TO-500	5	252 [133]	not detected	252	
2	Cs <sub>0.67</sub> TO-400	15	397 [152]	60 [557]	458	
3a	$Cs_{0.7}ZnTO-300$	6	100 [139]	108 [421]	206	
3b	$Cs_{0.7}ZnTO-400$	6	74 [148]	61 [566]	135	
3c	$Cs_{0.7}ZnTO-500$	6	66 [145]	6 [586]	72	
4	$K_{0.8}ZnTO-400$	3	not detected	not detected	not detected	
5a	$TiO_2$ -400	6	60 [126]	not detected	60	
5b	$TiO_2$ -700	6	56 [132]	not detected	56	
6	$H_{0.7}TO-400$	not available	133 [121]	178 [512]	311	
7	HZSM-5-400	350	361 [150]	30 [400]	392	

 ${}^a\mathrm{Cs_xTO}$  (Cs<sub>x</sub>Ti<sub>2-x/4</sub> $\square_{x/4}\mathrm{O_4}$ , where x=0.67 and 0.70), Cs<sub>0.7</sub>ZnTO (Cs<sub>0.7</sub>Zn<sub>0.35</sub>Ti<sub>1.65</sub> $\mathrm{O_4}$ ),  $\mathrm{K_{0.8}ZnTO}$  (K<sub>0.8</sub>Zn<sub>0.4</sub>Ti<sub>1.6</sub> $\mathrm{O_4}$ ), and H<sub>0.7</sub>TO (H<sub>0.7</sub>Ti<sub>1.825</sub> $\square_{0.175}\mathrm{O_4}$ ·H<sub>2</sub>O). The number after the name indicates the activation temperature  $T_a$  (in degrees Celsius) prior to NH<sub>3</sub> adsorption.

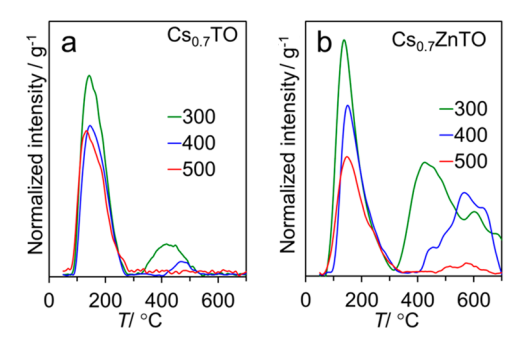


**Figure 6.** Temperature profiles of desorption of NH<sub>3</sub> from (a)  $Cs_{0.7}TO$  and (b)  $Cs_{0.7}ZnTO$  activated at  $T_a$  values of 300, 400, and 500 °C. Each profile was normalized by the mass of the sample.

and in Table 2 (entries 3a-3c). In fact, the decrease in total acidity upon Zn substitution is due to a notable decrease in LT acidity, which is accompanied by a moderate increase in HT acidity. This result suggests that Ti atoms at the proximity of the vacancy sites could be specifically responsible for NH<sub>3</sub> LT desorption. (The formation of hydroxylated groups due to water adsorption around the  $\square$  sites is energetically favorable;  $^{52,53}$  however, the adsorption of NH<sub>3</sub> has not been reported to the best of our knowledge.) Importantly, the observed increase in acidity upon HT desorption in Cs<sub>0.7</sub>ZnTO indicates the presence of other types of acid sites, which are not associated with the  $\square$  sites (also see the XPS results below).

The acidic nature of the cesium titanate microcrystals reported here suggests the novel bifunctional property of these materials, because only the basic nature of the lattice oxygen has been reported so far for lepidocrocite-type  $K_x M_y Ti_{2-y} O_4$ .  $^{36,38}$  The  $CO_2$  TPD measurements were performed, and the results are summarized in Figure S2 and Table S2. Although  $Cs_{0.7}TO$  exhibits a typical basicity, the (desorbed NH<sub>3</sub>)/(desorbed CO<sub>2</sub>) ratio that approximately represents the contribution of acidic to basic sites is 1.6. This ratio as determined in a similar manner for  $Cs_{0.7}ZnO$  is 2.9. Clearly, these numbers are significantly higher than that of  $TiO_2$  (0.9). Again, this result emphasizes the unusually acidic nature of the lepidocrocite-type cesium titanate, contrasting the basic site-dominating surfaces in other titanates such as the ATiO<sub>3</sub> (A = Sr or Ba) perovskite.  $^{54}$ 

The essential influence of polarizable  $Cs^+$  ions toward the acidic properties is further emphasized by comparing the  $\square$ -free  $Cs_{0.7}ZnTO$  ( $Cs_{0.7}Zn_{0.35}Ti_{1.65}O_4$ ; space group Immm;  $^{21}S_{BET}=6$  m $^2\cdot g^{-1}$ ) to  $K_{0.8}ZnTO$  [ $K_{0.8}Zn_{0.4}Ti_{1.6}O_4$ ; space group  $Cm2c_1$ ;  $^{19}S_{BET}=3$  m $^2$  g $^{-1}$  (Figure S1b)]. It is clear that, while  $Cs_{0.7}ZnTO$  shows considerable  $NH_3$  adsorption/desorption, the  $NH_3$  adsorption/desorption from  $K_{0.8}ZnTO$  was completely diminished, resulting in a flat TPD profile (not shown). This point will be discussed below with regard to the nature of the acid sites.

Altogether, while the  $S_{\rm BET}$  of the cesium titanate is rather low and has not yet been optimized, their acidity is comparable to that of typical acid zeolites  $^{55-57}$  or some high-acidity protonic titanate samples  $^{9,11,12}$  with a much larger  $S_{\rm BET}$ . This is rather exceptional because our samples are in the form of microcrystals—without the need for lengthy protonation/ion exchange, pillaring, delamination, or restacking—and have virtually no porosity. Additional examples comparing the acidic strength and acidity in our samples versus those reported in the literature can be found in Table S1.

**Possible Nature of Acid Sites.** Figure 7 shows the IR spectra of pyridine-sorbed  $Cs_{0.7}TO$  and  $Cs_{0.7}ZnTO$ . The

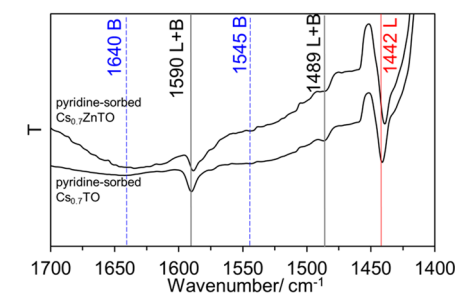


**Figure 7.** ATR spectra of pyridine-sorbed Cs<sub>0.7</sub>TO and Cs<sub>0.7</sub>ZnTO with the vibrations characteristic of pyridine adsorbed on Lewis (L), Brønsted (B), or the combination of these two sites (L+B) indicated.

strong peak at ~1440 cm<sup>-1</sup> typical of pyridine bound to Lewis acid sites 14,58 is clearly observed. On the contrary, the signal characteristics of pyridine bound to Brønsted acid sites is absent in these two samples. For K<sub>0.8</sub>ZnTO, we can observe only vibrations due to the titanate itself, without any signal due to sorbed pyridine. This result is in good agreement with the flat NH<sub>3</sub> TPD profile mentioned previously. In addition, the TPD experiment with isopropylamine that is specific to Brønsted acid sites<sup>31,32</sup> also showed virtually zero adsorption/desorption (not shown). Accordingly, one can deduce that Cs<sub>0.7</sub>TO and Cs<sub>0.7</sub>ZnTO are the Lewis acids. Because the interlayer Cs+ ions cannot be the Lewis acid center, it is most likely that the Ti<sup>4+</sup>/M<sup>n+</sup> ions on the accessible surfaces of the sheets (i.e., basal plane or edges) are the acid sites. However, our attempt to detect the surface Ti species by DRUV was unsuccessful, likely due to the small  $S_{\rm BET}$  of the samples and consequently the small amount of such species. A careful surface-sensitive analysis will be further required, which will provide not only the information about the local structure but also the possible correlation (if any) with catalytic activities in the future contribution.

Accordingly, the Ti 2p XPS spectra of some samples were recorded and are compared in Figure 8. Note that the Ti 2p signals are the average of all surface Ti species probed (analysis area of 300  $\mu$ m  $\times$  300  $\mu$ m), including Ti at the proximity of  $\square$ (and Zn) and Ti that is away from it. In all cases, the binding energy indicates the presence of  $Ti^{4+}$  as anticipated.  $^{21,22,49,59,60}$  Specifically, the  $\square$ -containing  $Cs_{0,7}TO$  shows the peaks at 459.3 eV (Ti  $2p_{3/2}$ ) and 465.0 eV (Ti  $2p_{1/2}$ ), which are more positive by ~1 eV than the corresponding signals in TiO<sub>2</sub> (458.4 and 464.1 eV, respectively). In the Zn-substituted Cs<sub>0.7</sub>ZnTO, the Ti 2p signals at binding energies (459.3 and 465.1 eV) similar to those of Cs<sub>0.7</sub>TO were observed. (The presence of another component at 457.8 and 463.5 eV might also suggest other sorts of acid sites.) The electropositive nature of surface Ti atoms in Cs<sub>0.7</sub>TO and Cs<sub>0.7</sub>ZnTO in relation to TiO<sub>2</sub> agrees qualitatively with the results from NH<sub>3</sub> TPD (Figure 5). For K<sub>0.8</sub>ZnTO,<sup>22</sup> the majority of the Ti 2p peak (458.1 eV, Ti  $2p_{3/2}$ ; 463.8 eV, Ti  $2p_{1/2}$ ) is close to that in TiO2. Clearly, the surface Ti species in K0.8ZnTO are not as electropositive as those in Cs<sub>0.7</sub>TO and Cs<sub>0.7</sub>ZnTO. The notable difference in the binding energies of Ti 2p in Cs<sub>0.7</sub>ZnTO and K<sub>0.8</sub>ZnTO might be related to the type of interlayer cation, composition, and also space group. (The latter can be seen from the XRD pattern in Figure 2 vs Figure

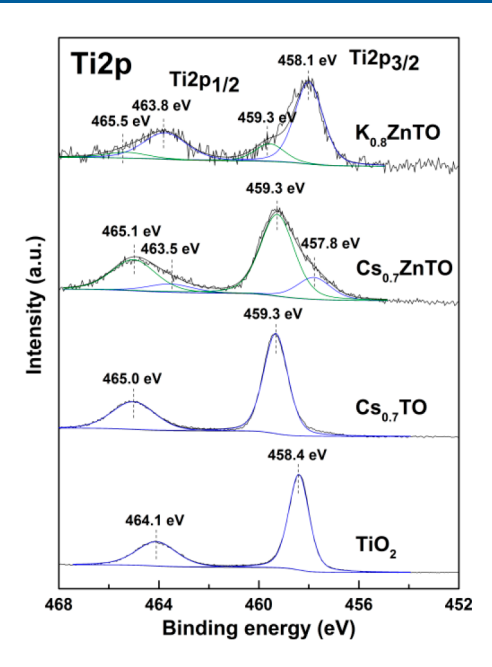


**Figure 8.** Ti 2p XPS spectra of anatase-type  $TiO_2$ ,  $Cs_{0.7}TO$ ,  $Cs_{0.7}ZnTO$ , and  $K_{0.8}ZnTO$ .

S1b, where the peak with the highest intensity is from the different hkl index.) A better understanding might be obtained by studying the compositions with mixed interlayer alkali ions (i.e.,  $Cs_{0.7-x}K_xZn_{0.35}Ti_{1.65}O_4$  vs  $Cs_{0.7}Zn_{0.35}Ti_{1.65}O_4$ ); this is being investigated.

The relative distribution of  $Ti^{4+}$  might be indirectly inferred from the compositional analyses of the  $Cs_{0.7}TO$  microcrystals (i.e.,  $Cs_{0.7}Ti_{1.825}\square_{0.175}O_4$ ) where the nominal Ti/Cs ratio equals 2.60. The surface Ti/Cs ratio (as determined by XPS) was 4.1  $\pm$  0.5, larger than that in the bulk (2.94  $\pm$  0.02 for XRF and 2.9  $\pm$  0.2 for EDX). That is, Ti termination and/or surface Ti enrichment was observed in  $Cs_{0.7}TO$ , potentially rendering the acidic character. For  $Cs_{0.7}ZnTO$  ( $Cs_{0.7}Zn_{0.35}Ti_{1.65}O_4$ ), the (Ti+Zn)/Cs ratios obtained from different techniques were similar: 2.86 (nominal value), 2.90 (XRF), 2.95 (EDX), and 2.30 (XPS). This result suggests a more homogeneous distribution of elements on the surface and in the bulk of  $Cs_{0.7}ZnO$ .

Similar analyses were conducted on the  $K_{0.8}ZnTO$ , but it was found that the surface of this material lacks Ti and Zn. This statement was deduced from the surface (Ti+Zn)/K ratio that is as low as 1.50,  $^{22}$  compared to the nominal value of 2.5 for  $K_{0.8}Zn_{0.4}Ti_{1.6}O_4$ .

The low concentration of surface Ti (and Zn) in the non-acidic  $K_{0.8}$ ZnTO contrasts with the high concentration of surface Ti in  $Cs_{0.7}$ TO or the homogeneous distribution of elements in  $Cs_{0.7}$ ZnTO. This result hints at the essential role of the large and polarizable  $Cs^+$  ions in the interlayer space toward surface relaxation, in combination with the presence of the Ti vacancy sites  $\square$  and/or the substituted atom. Note that this is the surface characteristic only, because XRD and Raman spectroscopy have already confirmed the preservation of the lepidocrocite structure at long and short range, respectively.

**Catalytic Activity.** Ethanol was employed as another probe molecule to further illustrate the dominating acid character in the lepidocrocite-type cesium titanate; acid sites convert ethanol to ethylene and diethyl ether, <sup>61,62</sup> while acid—base pairs couple two molecules of ethanol into butanol (i.e.,

Guebert reaction).  $^{63,64}$  The acidic  $Cs_{0.7}TO$  was chosen as a representative sample, in comparison to MgO, which is well-known to predominantly exhibit a basic character. Ethanol conversion and product yields as a function of time on stream in a flow reactor at 380  $^{\circ}C$  are shown in Figure 9.

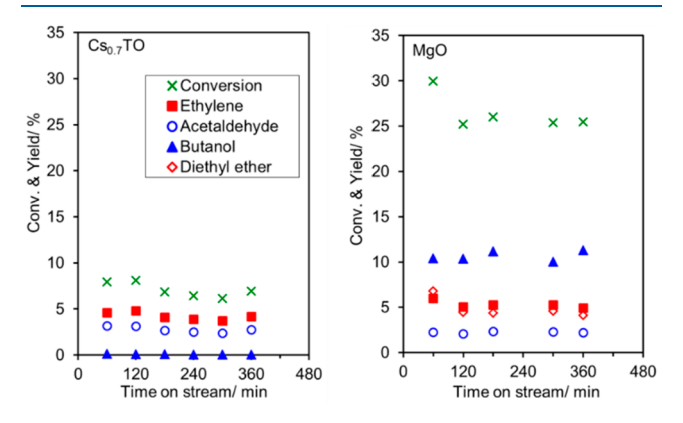


**Figure 9.** Conversion of ethanol and the percent yield of products over  $Cs_{0.7}TO$  (left) and MgO (right). Reaction conditions: activation in air at 400 °C for 2 h, reaction temperature of 380 °C, contact time of 58 g h mol<sup>-1</sup>, atmospheric pressure, and flow rate of carrier gas  $(N_2)$  of 60 mL min<sup>-1</sup>.

The initial conversion is 7.1% ( $Cs_{0.7}TO$ ) versus 30.0% (MgO), which can be ascribed to the difference in  $S_{BET}$  (5 m<sup>2</sup> g<sup>-1</sup> vs 63 m<sup>2</sup> g<sup>-1</sup>), suggesting that the observed catalytic activity is contributed mainly by the external surfaces. Notably, the major product over  $Cs_{0.7}TO$  is ethylene, which could be formed over acid sites. On the other hand, butanol, which is collectively formed over acid—base pairs, is the major product over MgO. (The yield of butanol is ~0.1% over  $Cs_{0.7}TO$ .) Clearly, the relative abundance of acidic to basic sites dictates the product distribution. A full account of catalytic activity measurements will be reported elsewhere.

Figure S1c compares the XRD patterns of the  $Cs_{0.7}TO$  before and after use (" $Cs_{0.7}TO$ -Spent") as a catalyst in this reaction. The layer structure is retained despite a halo and the slight peak broadening and/or a reduction in crystallite size (D=26 nm). This is presumably due to the partial desegregation of some microcrystal layers by water (i.e., steaming) produced in situ via ethanol dehydration, yet the possibility of using  $Cs_{0.7}TO$  at a reaction temperature as high as 380 °C greatly expands the temperature limit from that typically employed 12–16 in the protonic form (<100 °C).

#### CONCLUSION

In conclusion, we showed that  $Cs_xTi_{2-y}M_yO_4$  (x=0.67 or 0.70;  $M=\Box$  or Zn) microcrystals were unusually acidic as compared to common metal oxides. This is exceptional for layered metal oxides because (i) protonation/ion exchange, pillaring, delamination, restacking, or lengthy synthetic procedures are not required, (ii) cesium ions that are typically regarded as the promoter for basic character indeed enhance acidic character, and (iii) the microcrystals have a small  $S_{\rm BET}$ . The Lewis acidic nature was confirmed by IR of sorbed pyridine and very likely is related to the distribution of  $Ti^{4+}/M^{n+}$  species on the surface as suggested by XPS. Meanwhile, the acidity depends on several factors, including the presence of Ti vacancy  $\Box$ , the inductive effect of M (i.e., Zn),  $S_{\rm BET}$ , and the activation temperature. The soft and polarizable cesium

ions (but not the potassium analogue) were found to be essential in this unusually acidic nature. The production of ethylene from ethanol over  $Cs_{0.7}TO$  supports the presence of active acid sites. Importantly, the lepidocrocite-type layered structure is preserved after 700 °C, contrasting the conversion to anatase at the early temperature of 450 °C in the protonic analogue. The question of whether related structures  $^{37,65,66}$  (i.e., with variations in the number of repeating edge-shared octahedra) will exhibit this unusually acidic property, including the rationale behind such behavior, is interesting.

#### ASSOCIATED CONTENT

#### **S** Supporting Information

The Supporting Information is available free of charge on the ACS Publications website at DOI: 10.1021/acs.inorg-chem.9b00369.

Characterization, additional XRD patterns, table of acidities, CO<sub>2</sub> TPD profiles, and basicities (PDF)

#### AUTHOR INFORMATION

#### **Corresponding Authors**

\*E-mail: tosapol.ma@kmitl.ac.th. Telephone: +66 9 0992 2076. Fax: +66 2 329 8265.

\*E-mail: kstawan@gmail.com. Telephone: +66 8 1929 8288. Fax: +66 2 326 4415.

#### ORCID ®

Tosapol Maluangnont: 0000-0002-6213-5539

#### Notes

The authors declare no competing financial interest.

#### ACKNOWLEDGMENTS

This work was financially supported by the Thailand Research Fund (MRG6080004). The assistance of Korawich Trangwachirachai and Kittipong Prakobtham (isopropylamine TPD) is gratefully acknowledged. T.M. thanks Dr. Adisak Boonchun (Kasetsart University) for fruitful discussion.

#### REFERENCES

- (1) Busca, G. Acid catalysts in industrial hydrocarbon chemistry. *Chem. Rev.* **2007**, *107*, 5366–5410.
- (2) Zhou, C.-H.; Xia, X.; Lin, C.-X.; Tong, D.-S.; Beltramini, J. Catalytic conversion of lignocellulosic biomass to fine chemicals and fuels. *Chem. Soc. Rev.* **2011**, *40*, 5588–5617.
- (3) Helwani, Z.; Othman, M. R.; Aziz, N.; Kim, J.; Fernando, W. J. N. Solid heterogeneous catalysts for transesterification of triglycerides with methanol: A review. *Appl. Catal., A* **2009**, *363*, 1–10.
- (4) Su, F.; Guo, Y. Advancements in solid acid catalysts for biodiesel production. *Green Chem.* **2014**, *16*, 2934–2957.
- (5) Takagaki, A.; Tagusagawa, C.; Hayashi, S.; Hara, M.; Domen, K. Nanosheets as highly active solid acid catalysts for green chemical syntheses. *Energy Environ. Sci.* **2010**, *3*, 82–93.
- (6) Bavykin, D. V.; Friedrich, J. M.; Walsh, F. C. Protonated titanates and  ${\rm TiO_2}$  nanostructured materials: Synthesis, properties, and applications. *Adv. Mater.* **2006**, *18*, 2807–2824.
- (7) Tagusagawa, C.; Takagaki, A.; Hayashi, S.; Domen, K. Characterization of HNbWO<sub>6</sub> and HTaWO<sub>6</sub> metal oxide nanosheet aggregates as solid acid catalysts. *J. Phys. Chem. C* **2009**, *113*, 7831–7837.
- (8) Kooli, F.; Sasaki, T.; Watanabe, M.; Martin, C.; Rives, V. Microporosity and acidity properties of alumina pillared titanates. *Langmuir* **1999**, *15*, 1090–1095.
- (9) Kooli, F.; Sasaki, T.; Mizukami, F.; Watanabe, M.; Martin, C.; Rives, V. Characterization and acidic properties of silica pillared titanates. *J. Mater. Chem.* **2001**, *11*, 841–845.

(10) Maluangnont, T.; Matsuba, K.; Geng, F.; Ma, R.; Yamauchi, T.; Sasaki, T. Osmotic swelling of layered compounds as a route to producing high-quality two-dimensional materials. A comparative study of tetramethylammonium versus tetrabutylammonium cation in a lepidocrocite-type titanate. *Chem. Mater.* **2013**, 25, 3137–3146.

- (11) Lee, M.; Seo, Y.; Shin, H. S.; Jo, C.; Ryoo, R. Anatase  ${\rm TiO_2}$  nanosheets with surface acid sites for Friedel-Crafts alkylation. *Microporous Mesoporous Mater.* **2016**, 222, 185–191.
- (12) Kitano, M.; Nakajima, K.; Kondo, J. N.; Hayashi, S.; Hara, M. Protonated titanate nanotubes as solid acid catalyst. *J. Am. Chem. Soc.* **2010**, 132, 6622–6623.
- (13) Kitano, M.; Wada, E.; Nakajima, K.; Hayashi, S.; Miyazaki, S.; Kobayashi, H.; Hara, M. Protonated titanate nanotubes with Lewis and Brønsted acidity: relationship between nanotube structure and catalytic activity. *Chem. Mater.* **2013**, *25*, 385–393.
- (14) Wada, E.; Kitano, M.; Nakajima, K.; Hara, M. Effect of preparation conditions on the structural and acid catalytic properties of protonated titanate nanotubes. *J. Mater. Chem. A* **2013**, *1*, 12768–12774.
- (15) Kitano, M.; Kobayashi, H.; Hayashi, S.; Hara, M. Acid properties of protonated titanate nanotubes. *J. Jpn. Pet. Inst.* **2017**, *60*, 113–120.
- (16) de Carvalho, D. C.; Oliveira, A. C.; Ferreira, O. P.; Filho, J. M.; Tehuacanero-Cuapa, S.; Oliveira, A. C. Titanate nanotubes as acid catalysts for acetalization of glycerol with acetone: influence of the synthesis time and the role of structure on the catalytic performance. *Chem. Eng. J.* **2017**, *313*, 1454–1467.
- (17) Sasaki, T.; Watanabe, M.; Michiue, Y.; Komatsu, Y.; Izumi, F.; Takenouchi, S. Preparation and acid-base properties of a protonated titanate with the lepidocrocite-like layer structure. *Chem. Mater.* **1995**, 7, 1001–1007.
- (18) Grey, I. E.; Li, C.; Madsen, I. C.; Watts, J. A. The stability and structure of  $Cs_x[Ti_{2-x/4} \square_{x/4}] O_4$ , 0.61 < x < 0.65. *J. Solid State Chem.* **1987**, 66, 7–19.
- (19) Groult, D.; Mercey, C.; Raveau, B. Nouveaux oxydes à structure en feuillets: Les titanates de potassium non-stoechiométriques  $K_x(M_vTi_{2-v})O_4$ . J. Solid State Chem. 1980, 32, 289–296.
- (20) Reid, A. F.; Mumme, W. G.; Wadsley, A. D. A new class of compound  $M_x^+ A_x^{3+} Ti_{2-x} O_4$  (0.60 < x < 0.80) typified by  $Rb_x Mn_x Ti_{2-x} O_4$ . Acta Crystallogr., Sect. B: Struct. Crystallogr. Cryst. Chem. 1968, B24, 1228–1233.
- (21) Gao, T.; Fjellvåg, H.; Norby, P. Defect chemistry of a zinc-doped lepidocrocite titanate  $Cs_xTi_{2-x/2}Zn_{x/2}O_4$  (x=0.7) and its protonic form. *Chem. Mater.* **2009**, 21, 3503–3513.
- (22) Maluangnont, T.; Chanlek, N.; Suksawad, T.; Tonket, N.; Saikhamdee, P.; Sukkha, U.; Vittayakorn, N. Beyond soft chemistry bulk and surface modifications of polycrystalline lepidocrocite titanate induced by post-synthesis thermal treatment. *Dalton Trans.* **2017**, *46*, 14277–14285.
- (23) Momma, K.; Izumi, F. VESTA 3 for three-dimensional visualization of crystal, volumetric and morphology data. *J. Appl. Crystallogr.* **2011**, *44*, 1272–1276.
- (24) Yokosawa, K.; Takei, T.; Yanagida, S.; Kumada, N.; Katsumata, K. Ion exchange of layered titanate with transition metal and application to ammonia storage. *J. Ceram. Soc. Jpn.* **2018**, 126, 808–813
- (25) Camposeco, R.; Castillo, S.; Mejia-Centeno, I.; Navarrete, J.; Rodriguez-Gonzalez, V. Behavior of Lewis and Brönsted surface acidity featured by Ag, Au, Ce, La, Fe, Mn, Pd, Pt, V and W decorated on protonated titanate nanotubes. *Microporous Mesoporous Mater.* **2016**, 236, 235–243.
- (26) Srilatha, K.; Sree, R.; Prabhavathi Devi, B. L. A.; Sai Prasad, P. S.; Prasad, R. B. N.; Lingaiah, N. Preparation of biodiesel from rice bran fatty acids catalyzed by heterogeneous cesium-exchanged 12-tungstophosphoric acids. *Bioresour. Technol.* **2012**, *116*, 53–57.
- (27) Sararuk, C.; Yang, D.; Zhang, G.; Li, C.; Zhang, S. One-step aldol condensation of ethyl acetate with formaldehyde over Ce and P modified cesium supported alumina catalyst. *Ind. Eng. Chem.* **2017**, 46, 342–349.

(28) Li, J.; Davis, R. J. On the use of 1-butene double-bond isomerization as a probe reaction on cesium-loaded zeolite X. *Appl. Catal.*, A 2003, 239, 59–70.

- (29) Davis, R. J. New perspectives on basic zeolites as catalysts and catalyst supports. *J. Catal.* **2003**, *216*, 396–405.
- (30) Jiang, X.; Manawan, M.; Feng, T.; Qian, R.; Zhao, T.; Zhou, G.; Kong, F.; Wang, Q.; Dai, S.; Pan, J. H. Anatase and rutile in Evonik aroxide P25: Heterojunctioned or individual nanoparticles? *Catal. Today* **2018**, *300*, 12–17.
- (31) Kofke, T. J. G.; Gorte, R. J.; Farneth, W. E. Stoichiometric adsorption complexes in H-ZSM-5, H-ZSM-12, and H-Mordenite zeolites. *J. Catal.* **1989**, *115*, 265–272.
- (32) Parrillo, D. J.; Adamo, A. T.; Kokotailo, G. T.; Gorte, R. J. Amine adsorption in H-ZSM-5. *Appl. Catal.* **1990**, *67*, 107–118.
- (33) Eun Ko, J.; Jin Kwon, B.; Jung, H. Synthesis and characterization of the SnO<sub>2</sub>-pillared layered titanate nanohybrid. *J. Phys. Chem. Solids* **2010**, *71*, 658–662.
- (34) Choy, J.-H.; Lee, H.-C.; Jung, H.; Kim, H.; Boo, H. Exfoliation and restacking route to anatase-layered titanate nanohybrid with enhanced photocatalytic activity. *Chem. Mater.* **2002**, *14*, 2486–2491.
- (35) Miura, H. CellCalc: A unit cell parameter refinement program on Windows computer. *Nippon Kessho Gakkaishi* **2003**, *45*, 145–147. (in Japanese)
- (36) Maluangnont, T.; Arsa, P.; Limsakul, K.; Juntarachairot, S.; Sangsan, S.; Gotoh, K.; Sooknoi, T. Surface and interlayer base-characters in lepidocrocite titanate: The adsorption and intercalation of fatty acid. *J. Solid State Chem.* **2016**, 238, 175–181.
- (37) Sasaki, T.; Komatsu, Y.; Fujiki, Y. Protonated pentatitanate: preparation, characterizations and cation intercalation. *Chem. Mater.* **1992**, *4*, 894–899.
- (38) Maluangnont, T.; Arsa, P.; Sooknoi, T. Extending the basic function of lattice oxygen in lepidocrocite titanate the conversion of intercalated fatty acid to liquid hydrocarbon fuels. *J. Solid State Chem.* **2017**, 256, 219–226.
- (39) Dong, X.; Osada, M.; Ueda, H.; Ebina, Y.; Kotani, Y.; Ono, K.; Ueda, S.; Kobayashi, K.; Takada, K.; Sasaki, T. Synthesis of Mnsubstituted titania nanosheets and ferromagnetic thin films with controlled doping. *Chem. Mater.* **2009**, *21*, 4366–4373.
- (40) Song, H.; Sjåstad, A. O.; Vistad, Ø. B.; Gao, T.; Norby, P. Preparation of Nb-substituted titanates by a novel sol-gel assisted solid state reaction. *Inorg. Chem.* **2009**, *48*, 6952–6959.
- (41) Gao, T.; Fjellvag, H.; Norby, P. Crystal structures of titanate nanotubes: a Raman scattering study. *Inorg. Chem.* **2009**, *48*, 1423–1432.
- (42) Gao, T.; Fjellvag, H.; Norby, P. Raman scattering properties of a protonic titanate  $H_xTi_{2-x/4} \square_{x/4} O_4 \cdot H_2O$  ( $\square$ , vacancy; x = 0.7) with lepidocrocite-type layered structure. *J. Phys. Chem. B* **2008**, *112*, 9400–9405.
- (43) Adar, F. Molecular spectroscopy workbench Raman spectra of metal oxides. *Spectroscopy* **2014**, *29*, 14.
- (44) Kouva, S.; Kanervo, J.; Schüβler, F.; Olindo, R.; Lercher, J. A.; Krause, O. Sorption and diffusion parameters from vacuum-TPD of ammonia on H-ZSM-5. *Chem. Eng. Sci.* **2013**, *89*, 40–48.
- (45) Gorte, R. J. Temperature-programmed desorption for the characterization of oxide catalysts. Catal. Today 1996, 28, 405-414.
- (46) Gorte, R. J. Design parameters for temperature programmed desorption from porous catalysts. *J. Catal.* **1982**, *75*, 164–174.
- (47) Sanderson, R. T. Electronegativity and bond energy. J. Am. Chem. Soc. 1983, 105, 2259–2261.
- (48) Sanderson, R. T. Electronegativity and bonding of transitional elements. *Inorg. Chem.* **1986**, 25, 3518–3522.
- (49) Wang, H.; Song, Y.; Xiong, J.; Bi, J.; Li, L.; Yu, Y.; Liang, S.; Wu, L. Highly selective oxidation of furfuryl alcohol over monolayer titanate nanosheet under visible light irradiation. *Appl. Catal., B* **2018**, 224, 394–403.
- (50) Ohwada, M.; Kimoto, K.; Mizoguchi, T.; Ebina, Y.; Sasaki, T. Atomic structure of titania nanosheet with vacancies. *Sci. Rep.* **2013**, *3*, 2801.

(51) Ohwada, M.; Kimoto, K.; Suenaga, K.; Sato, Y.; Ebina, Y.; Sasaki, T. Synthesis and atomic characterization of a Ti<sub>2</sub>O<sub>3</sub> nanosheet. *J. Phys. Chem. Lett.* **2011**, *2*, 1820–1823.

- (52) Uchida, Y.; Hara, M.; Funatsu, A.; Shimojo, F. Electronic structure of titania nanosheets with vacancies based on first-principles calculations. *e-J. Surf. Sci. Nanotechnol.* **2018**, *16*, 1–4.
- (53) Grey, I. E.; Wilson, N. C. Titanium vacancy defects in sol-gel prepared anatase. *J. Solid State Chem.* **2007**, *180*, 670–678.
- (54) Foo, G. S.; Polo-Garzon, F.; Fung, V.; Jiang, D.-E.; Overbury, S. H.; Wu, Z. Acid-base reactivity of perovskite catalysts probed via conversion of 2-propanol over titanates and zirconates. *ACS Catal.* **2017**, *7*, 4423–4434.
- (55) Al-Dughaither, A. S.; de Lasa, H. HZSM-5 zeolites with different SiO<sub>2</sub>/Al<sub>2</sub>O<sub>3</sub> ratios. Characterization and NH<sub>3</sub> desorption kinetics. *Ind. Eng. Chem. Res.* **2014**, *53*, 15303–15316.
- (56) Kapustin, G. I.; Brueva, T. R.; Klyachko, A. L.; Beran, S.; Wichterlova, B. Determination of the number and acid strength of acid sites in zeolites by ammonia adsorption. Comparison of calorimetry and temperature-programmed desorption of ammonia. *Appl. Catal.* 1988, 42, 239–246.
- (\$7) Shetsiri, S.; Thivasasith, A.; Saenluang, K.; Wannapakdee, W.; Salakhum, S.; Wetchasat, P.; Nokbin, S.; Limtrakul, J.; Wattanakit, C. Sustainable production of ethylene from bioethanol over hierarchical ZSM-5 nanosheets. *Sustainable Energy Fuels* **2019**, *3*, 115–126.
- (58) Bezrodna, T.; Puchkovska, G.; Shimanovska, V.; Chashechnikova, I.; Khalyavka, T.; Baran, J. Pyridine-TiO<sub>2</sub> surface interaction as a probe for surface active centers analysis. *Appl. Surf. Sci.* **2003**, *214*, 222–231.
- (59) Gao, T.; Norby, P.; Okamoto, H.; Fjellvåg, H. Syntheses, structures, and magnetic properties of nickel-doped lepidocrocite titanates. *Inorg. Chem.* **2009**, *48*, 9409–9418.
- (60) Pilarski, M.; Marschall, R.; Gross, S.; Wark, M. Layered cesium copper titanate for photocatalytic hydrogen production. *Appl. Catal., B* **2018**, 227, 349–355.
- (61) Aitchison, H.; Wingad, R. L.; Wass, D. F. Homogeneous ethanol to butanol catalysis—Guerbet renewed. ACS Catal. 2016, 6, 7125–7132.
- (62) Zhang, M.; Yu, Y. Dehydration of ethanol to ethylene. *Ind. Eng. Chem. Res.* **2013**, 52, 9505–9514.
- (63) Sun, J.; Wang, Y. Recent advances in catalytic conversion of ethanol to chemicals. ACS Catal. 2014, 4, 1078–1090.
- (64) Idriss, H.; Seebauer, E. G. Reactions of ethanol over metal oxides. J. Mol. Catal. A: Chem. 2000, 152, 201–212.
- (65) Sasaki, T.; Komatsu, Y.; Fujiki, Y. Rb<sup>+</sup> and Cs<sup>+</sup> incorporation mechanism and hydrate structures of layered hydrous titanium dioxide. *Inorg. Chem.* **1989**, 28, 2776–2779.
- (66) Kwiatkowska, J.; Grey, I. E.; Madsen, I. C.; Bursill, L. A. An X-ray and neutron diffraction study of  $Cs_2Ti_5O_{11}$  and  $Cs_2Ti_5O_{11}X_2O$ , X = H, D. Acta Crystallogr., Sect. B: Struct. Sci. 1987, B43, 258–265.

A2. แบบสรุปปิดโครงการและการนำผลจากโครงการไปใช้ประโยชน์

## รายงานสรุปการนำผลงานวิจัยไปใช้ประโยชน์

สัญญาเลขที่ MRG6080004 ชื่อโครงการ การผลิตเอทิลีนหรือบิวทานอลจากเอทานอลชีวภาพด้วยสมบัติกรดเบสของ				
เลพิโดโครไซท์ไททาเ	เนท หัวหน้า	<b>โครงการ</b> ผศ.ดร. ทศพล เมลืองนนท์ <b>หน่วยงาน</b> วิทยาลัยนาโนเทคโนโลยีพระจอมเกล้าลาดกระบัง		
สถาบันเทคโนโลยีพระจอมเกล้าเจ้าคุณทหารลาดกระบัง <b>โทรศัพท์</b> 02 329 8000 ต่อ 2134 <b>โทรสาร</b> 02 329 8265				
อีเมล์ tosapol.ma@kmitl.ac.th				
สถานะผลงาน □	ปกปิด	🗹 ไม่ปกปิด		

### ความสำคัญ / ความเป็นมา

The conversion of ethanol to value-added chemicals such as ethylene or butanol is of interest. Common acidic materials catalyzing the ethanol-to-ethylene transformation include thermally <u>un</u>stable (<100 °C) protonic titanate. Meanwhile, titanate-based materials with basic sites for ethanol-to-butanol conversion are not well known. This project reported the cesium lepidocrocite titanates as the rare examples of acidic cesium-containing titanium oxides, capable of catalyzing the ethanol-to-ethylene transformation. This project is an exploration (but to different directions) from the previous TRG5780160 on the basic properties of potassium lepidocrocite titanate, for the production of diesel-like hydrocarbons from fatty acids.

### วัตถุประสงค์ของโครงการ

- 1. To synthesized selected compositions of alkali lepidocrocite titanate  $Cs_xTi_{2-x/4}$   $\square_{x/4}O_4$  (x = 0.70 and 0.67),  $Cs_xZn_{x/2}Ti_{2-x/2}O_4$  (x = 0.70) and  $K_xZn_{x/2}Ti_{2-x/2}O_4$  (x = 0.80).
- To characterize the prepared materials, i.e., local- and long-range structure, thermal stability, morphology, compositional distribution, and acidic-basic properties; and to compare the acidic properties with more widely-studied materials
- 3. To evaluate the catalytic activity of the synthesized materials in ethanol conversion; and to make a correlation to the characterized physicochemical properties

#### ผลการวิจัย

The unusually acidic nature of the title compounds is exceptional considering the ease of synthesis and the presence of Cs<sup>+</sup>, typically believed to promote basic character. No other cesium-containing oxides exhibit the acidic property to the best of the author's knowledge. The ethylene production from ethanol at 380 °C further confirms the acidic character. The rather low ethanol conversion (7-13%) can be improved by ball milling. Importantly, the lepidocrocite-type layered structure is preserved under harsh environment, opening up the possibility for other high-temperature application.

#### คำสืบค้น (Keywords)

Bioethanol เอทานอลชีวภาพ; ethylene เอทิลีน; lepidocrocite titanate เลพิโดโครไซท์ไททาเนท; acid strength and acidity ความแรง ของกรดและความเป็นกรด

การนำผลงานวิจัยไปใช้ประโยชน์ (ดูคำจำกัดความ และตัวอย่างด้านหลังแบบฟอร์ม)					
□ ด้านนโยบาย					
□ ด้านสาธารณะ	🗆 ด้านสาธารณะ				
🗆 ด้านชุมชนและพื้นที่	🗆 ด้านชุมชนและพื้นที่				
🗆 ด้านพาณิชย์					
🗹 ด้านวิชาการ	โดยหัวหน้าโครงการนำไปใช้เป็นตัวอย่างสอนนักศึกษาระดับปริญญาตรีและบัณฑิตศึกษา เผยแพร่ใน	งาน			
ประชุมวิชาการและวารสารทางวิชาการ และเป็นพื้นฐานสำหรับโครงการวิจัยในอนาคต					
🗆 ยังไม่มีการนำไปใช้ (โปรดกรอกในกรอบถัดไป)					

	<u>(กรณีที่ยังไม่มีการใช้ประโยชน์)</u> ผลงานวิจัยมีศักยภาพในการนำไปใช้ประโยชน์				
	🗆 ด้านนโยบาย 🗆 ด้านสาธารณะ 🗆 ด้านชุมชนและพื้นที่ 🗆 ด้านพาณิชย์ 🗆 ด้านวิชาการ				
ข้อ	เสนอแนะเพื่อให้ผลงานถูกนำไปใช้ประโยชน์				
กา	รเผยแพร่/ประชาสัมพันธ์ (กรุณาให้รายละเอียด พร้อมแนบหลักฐาน)				
	สิ่งพิมพ์ หรือสื่อทั่วไป				
	🗆 หนังสือพิมพ์ 🗅 วารสาร 🗆 โทรทัศน์ 🗅 วิทยุ 🗅 เว็บไซต์ 🗅 คู่มือ/แผ่นพับ 🗅 จัดประชุม/อบรม 🗅 อื่น ๆ				
2.	สิ่งพิมพ์ทางวิชาการ (วารสาร, การประชุม ให้ระบุรายละเอียดแบบการเขียนเอกสารอ้างอิง เพื่อการค้นหาซึ่งควรประกอบด้วย ชื่อผู้แต่ง ชื่อเรื่อง แหล่งพิมพ์ ปี พ.ศ. (ค.ศ.)  ฉบับที่  หน้า  )				
	Maluangnont, T.; Wuttitham, B.; Hongklai, P.; Khunmee, P.; Tippayasukho, S.; Chanlek, N.; Sooknoi, T. "An unusually				
	acidic and thermally stable cesium titanate $Cs_xTi_{2-y}MyO_4$ (x = 0.67 or 0.70; M = vacancy or Zn)" <i>Inorg. Chem.</i> <b>2019</b> , 58,				
	6885-6892. [2018 Impact Factor = 4.85; Q1 in Inorganic Chemistry; Q1 in Chemistry (miscellaneous)]				

A3. สรุปรายงานการเงิน

## สัญญาเลขที่ MRG6080004 โครงการ: การผลิตเอทิลีนหรือบิวทานอลจากเอทานอลชีวภาพ ด้วยสมบัติกรดเบสของเลพิโดโครไชท์ไททาเนท รายงานสรุปการเงินในรอบ 24 เดือน

รายงานในช่วงตั้งแต่วันที่	4/3/2560	ถึงวันที่	10/2/2562		
	<u>รายจ่าย</u>				
หมวด	รายจ่ายสะสม	ค่าใช้จ่าย	รวมรายจ่าย	งบประมาณ	คงเหลือ
(ตามสัญญา)	จากรายงาน ครั้งก่อน	งวดปัจจุบัน	สะสมจนถึง งวดปัจจุบัน	รวมทั้ง โครงการ	(หรือเกิน)
1. ค่าตอบแทน	234,000.00	0.00	234,000.00	312,000.00	78,000.00
2. ค่าจ้าง	0.00	0.00	0.00	0.00	0.00
3. ค่าวัสดุ	33,975.00	126,990.53	160,965.53	153,000.00	-7,965.53
4. ค่าใช้สอย	82,944.00	45,757.56	128,701.56	135,000.00	6,298.44
5. ค่าครุภัณฑ์	0.00	0.00	0.00	0.00	0.00
6	0.00	0.00	0.00	0.00	0.00
รวม	350,919.00	172,748.09	523,667.09	600,000.00	76,332.91
	ลำบาบเงิบเ	ที่ได้รับและจำนวนเ	เงิบดงบหลือ		
จำนวนเงินที่ได้รับ	416366061	TENTIL REMOVE LETTE	EO WHO EN INE		
งวดที่ 1		100,000.00	บาท	16/06/60	
งวดที่ 2		200,000.00		16/06/60	
งวดที่ 3		100,000.00		08/08/61	
งวดที่ 4		122,000.00		08/08/61	
ดอกเบี้ย ครั้งที่ 1		61.64		30/06/60	
ดอกเบี้ย ครั้งที่ 2		536.16		31/12/60	
ดอกเบี้ย ครั้งที่ 3		293.43	บาท	30/06/61	
ดอกเบี้ย ครั้งที่ 4		439.24	บาท	31/12/61	
ดอกเบี้ย ครั้งที่ 5		332.85	บาท	30/06/62	
ดอกเบี้ย ครั้งที่ 6		169.11	บาท	21/1/1900	
	รวม	523,832.43	บาท (A)		
		ค่าใช้	จ่าย		
งวดที่ 1		110,533.00		2/10/60	
งวดที่ 2		117,213.00		4/4/61	
งวดที่ 3		123,173.00		3/10/61	
งวดที่ 4		172,748.10	บาท	6/11/62	
งวดที่ 5		0.00	บาท	เมื่อ วันที่	
	รวม	523,667.10	บาท (B)		

ลงนามหัวหน้าโครงการวิจัยผู้รับทุน ลงนามเจ้าหน้าที่การเงินโครงการ

165.33 บาท

<u>หมายเหตุ</u> 1. **ตัวเลขใน cell สีฟ้า** (ยอดรวมรายจ่ายสะสมจนถึงงวดปัจจุบันและยอดรวมค่าใช้จ่าย) **ต้องเท่ากัน**2. ยอดจำนวนเงินคงเหลือ (A-B) ควรเท่ากับหรือใกล้เคียงกับยอดคงเหลือในสำเนาสมุดบัญชี

จำนวนเงินคงเหลือ (A-B)

A4. หนังสือนำส่งรายงานฉบับสมบูรณ์

ที่ อว 7023/0354



วิทยาลัยนาโนเทคโนโลยีพระจอมเกล้าลาดกระบัง สถาบันเทคโนโลยีพระจอมเกล้าเจ้าคุณทหารลาดกระบัง ถนนฉลองกรุง เขตลาดกระบัง กรุงเทพฯ 10520

11 ตุลาคม 2562

**เรื่อง** รายงานฉบับสมบูรณ์โครงการวิจัย

เรียน ผู้อำนวยการสำนักงานคณะกรรมการส่งเสริมวิทยาศาสตร์วิจัยและนวัตกรรม

สิ่งที่ส่งมาด้วย รายงานฉบับสมบูรณ์ รหัสโครงการ MRG6080004

ตามที่ สำนักงานคณะกรรมการส่งเสริมวิทยาศาสตร์วิจัยและนวัตกรรม (สกสว.) ได้แจ้งผลการพิจารณา ทุนเห็นชอบในการสนับสนุนทุนส่งเสริมนักวิจัยรุ่นใหม่ ประจำปังบประมาณ 2560 เรื่อง "การผลิตเอทิลีนหรือบิวทา นอลจากเอทานอลชีวภาพด้วยสมบัติกรดเบสของเลพิโดโครไซท์ไททาเนต" สัญญาเลขที่ MRG6080004 ระยะเวลา 2 ปี (ตั้งแต่วันที่ 3 เมษายน 2560 ถึงวันที่ 2 เมษายน 2562) งบประมาณ 600,000 บาท โดยมี ผู้ช่วยศาสตราจารย์ ดร.ทศพล เมลืองนนท์ เป็นหัวหน้าโครงการวิจัย และได้ขอขยายระยะเวลาดำเนิน โครงการ ระยะเวลา 6 เดือน เนื่องจากต้องทำการทดลองและวิเคราะห์ผลเพิ่มเติม นั้น

บัดนี้ ผู้ช่วยศาสตราจารย์ ดร.ทศพล เมลืองนนท์ ได้ดำเนินโครงการวิจัยเสร็จเป็นที่เรียบร้อยแล้ว จึงมีความประสงค์ขอส่งรายงานฉบับสมบูรณ์ ตามสิ่งที่ส่งมาด้วยแล้วนี้

จึงเรียนมาเพื่อโปรดทราบและพิจารณา จะขอบพระคุณยิ่ง

ขอแสดงความนับถือ

(ผู้ช่วยศาสตราจารย์ ดร.วิภู ศรีสืบสาย)

คณบดี

วิทยาลัยนาโนเทคโนโลยีพระจอมเกล้าลาดกระบัง สจล. โทรศัพท์ 02-329-8000 ต่อ 3034 โทรสาร 02-329-8265

A5. หนังสือขออนุมัติเปลี่ยนชื่อโครงการ



ที่ นร6208/1268/2561

2 สิงหาคม 2561

เรื่อง อนุมัติปรับเปลี่ยนชื่อโครงการวิจัย เรียน ดร.ทศพล เมลืองนนท์

ตามที่ท่านได้รับทุนพัฒนาศักยภาพในการทำงานวิจัยของอาจารย์รุ่นใหม่ ประจำปี 2560 สัญญา เลขที่ MRG6080004 ระยะเวลาโครงการ 2 ปี ตั้งแต่วันที่ 3 เมษายน 2560 ถึงวันที่ 2 เมษายน 2562 และ ขออนุมัติปรับเปลี่ยนชื่อโครงการวิจัยจากเดิมคือ "การประยุกต์ใช้เลพิโดโครไซท์ไททาเนทนาโนชีทเป็นตัวเร่ง ปฏิกิริยาเพื่อการเปลี่ยนเอทานอลชีวภาพเป็นออกซิจิเนตที่ยาวกว่าห้าคาร์บอนอะตอม" ไปเป็น "การผลิต เอทิลีนหรือบิวทานอลจากเอทานอลชีวภาพด้วยสมบัติกรดเบสของเลพิโดโครไซท์ไททาเนท" นั้น

ฝ่ายวิชาการ สกว. พิจารณาแล้วอนุมัติตามที่ขอมา

จึงเรียนมาเพื่อทราบ

ขอแสดงความนับถือ

(ศ.ดร.สมปอง คล้ายหนองสรวง) ผู้อำนวยการฝ่ายวิชาการ สำนักงานกองทุนสนับสนุนการวิจัย

ฝ่ายวิชาการ สกว. โทรศัพท์ 0 2278 8200 ต่อ 8389 โทรสาร 0 2278 8248 E-mail: sutasinee@trf.or.th

"ค้าคุณต้อนการทำวิจัย...biodata ให้โอกาส เชิญสนทะเบียนรับทราบโจทย์วิจัย ที่ http://biodata.trf.or.th"

ชั้น 14 อาการ เอส เอ็ม ทาวเวอร์ 979/17-21 ถนนพหลโยธิน แขวงสามเสนใน เขตพญาไท กรุงเทพฯ 10400 14th Floor, S M Tower, 979/17-21 Phaholyothin Road, Samsennai, Phayathai, Bangkok 10400, Thailand Tel: +66 (0) 2278-8200 Fax: +66 (0) 2298-0476 http://www.trf.or.th E-mail: callcenter@trf.or.th

A6. หนังสือขออนุมัติขยายเวลาโครงการวิจัย

## สำนักงานคณะกรรมการส่งเสริมวิทยาศาสตร์ วิจัยและนวัตกรรม (สกสว.)

ชั้น ๑๔ อาคาร เอส เอ็ม ทาวเวอร์ ๙๗๙/๑๗ - ๒๑ ถนนพหลโยธิน แขวงสามเสนใน เขตพญาไท กรุงเทพฯ ๑๐๔๐๐ โทรศัพท์ ๐๒ – ๒๗๘ - ๘๒๐๐ โทรสาร ๐๒ - ๒๙๘ - ๐๔๗๖

ที่ อว.6309/0219/2562

14 พฤษภาคม 2562

เรื่อง อนุมัติขยายเวลาโครงการวิจัย เรียน ผศ.ดร.ทศพล เมลืองนนท์

ตามที่อาจารย์ได้รับทุนพัฒนาศักยภาพในการทำงานวิจัยของอาจารย์รุ่นใหม่ เรื่อง "การประยุกต์ใช้ เลพิโดโครไซท์ไททาเนทนาโนซีทเป็นตัวเร่งปฏิกิริยาเพื่อการเปลี่ยนเอทานอลชีวภาพเป็นออกซิจิเนตที่ยาวกว่าห้า คาร์บอนอะตอม" เลขที่สัญญา MRG6080004 มีกำหนดระยะเวลา 2 ปี และขออนุมัติขยายเวลาสิ้นสุด โครงการวิจัย 6 เดือน จากเดิมวันที่ 2 เมษายน พ.ศ. 2562 เป็นสิ้นสุดโครงการวันที่ 2 ตุลาคม พ.ศ. 2562

ฝ่ายวิชาการ สกสว. พิจารณาแล้วอนุมัติตามที่ได้แจ้งมา ทั้งนี้ขอให้หัวหน้าโครงการส่งรายงานฉบับสมบูรณ์ ตามเวลาที่กำหนด และหากมีข้อขัดข้องประการใดขอให้แจ้งมายังฝ่ายวิชาการ สกสว. ด้วย จักขอบคุณยิ่ง

จึงเรียนมาเพื่อทราบ

ขอแสดงความนับถือ

(ศ.ดร.สมปอง คล้ายหนองสรวง)
รองผู้อำนวยการด้านการวิจัยพื้นฐานและการพัฒนานักวิจัยและ
รักษาการผู้อำนวยการฝ่ายวิชาการ สกสว.

ฝ่ายวิชาการ สกว. โทรศัพท์ 0 2278 8200 ต่อ 8389 โทรสาร 0 2278 8248 Email: sutasinee@trf.or.th

A7. Permission/license to reproduce the published work















An Unusually Acidic and Thermally Stable Cesium Titanate CsxTi2-yMyO4 (x =

0.67 or 0.70; M = vacancy or

Zn)

**Author:** Tosapol Maluangnont,

Boonyawat Wuttitham, Panisa

Hongklai, et al

**Publication:** Inorganic Chemistry

**Publisher:** American Chemical Society

**Date:** May 1, 2019

Copyright © 2019, American Chemical Society

#### **LOGIN**

If you're a copyright.com user, you can login to RightsLink using your copyright.com credentials.

Already a RightsLink user or

want to <u>learn more?</u>

#### PERMISSION/LICENSE IS GRANTED FOR YOUR ORDER AT NO CHARGE

This type of permission/license, instead of the standard Terms & Conditions, is sent to you because no fee is being charged for your order. Please note the following:

- Permission is granted for your request in both print and electronic formats, and translations.
- If figures and/or tables were requested, they may be adapted or used in part.
- Please print this page for your records and send a copy of it to your publisher/graduate school.
- Appropriate credit for the requested material should be given as follows: "Reprinted (adapted) with permission from (COMPLETE REFERENCE CITATION). Copyright (YEAR) American Chemical Society." Insert appropriate information in place of the capitalized words.
- One-time permission is granted only for the use specified in your request. No additional
  uses are granted (such as derivative works or other editions). For any other uses, please
  submit a new request.

BACK

**CLOSE WINDOW** 

Copyright © 2019 Copyright Clearance Center, Inc. All Rights Reserved. Privacy statement. Terms and Conditions. Comments? We would like to hear from you. E-mail us at customercare@copyright.com